

## Energy Decay of the 2004 Sumatra Tsunami in the World Ocean

ALEXANDER B. RABINOVICH,<sup>1,2</sup> ROGÉRIO N. CANDELLA,<sup>3</sup> and RICHARD E. THOMSON<sup>1</sup>

**Abstract**—The catastrophic Indian Ocean tsunami generated off the coast of Sumatra on 26 December 2004 was recorded by a large number of tide gauges throughout the World Ocean. This study uses gauge records from 173 sites to examine the characteristics and energy decay of the tsunami waves from this event in the Indian, Atlantic and Pacific oceans. Findings reveal that the decay (*e*-folding) time of the tsunami wave energy within a given oceanic basin is not uniform, as previously reported, but depends on the absorption characteristics of the shelf adjacent to the coastal observation site and the time for the waves to reach the site from the source region. In general, the decay times for island and open-ocean bottom stations are found to be shorter than for coastal mainland stations. Decay times for the 2004 Sumatra tsunami ranged from about 13 h for islands in the Indian Ocean to 40–45 h for mainland stations in the North Pacific.

**Key words:** 2004 Sumatra tsunami, tsunami travel time, tsunami decay time, tsunami energy index, maximum wave heights, tide gauge data.

### 1. Introduction

The  $M_w = 9.3$  megathrust earthquake of 26 December 2004 off the coast of Sumatra generated a major tsunami that destructively impacted coastal regions in the Indian Ocean. This was the first global-scale tsunami to occur during the “instrumental era” and was recorded by a large number of tide gauges throughout the World Ocean (TITOV *et al.*, 2005; MERRIFIELD *et al.*, 2005; RABINOVICH *et al.*, 2006; LEONARD, 2006; RABINOVICH and THOMSON, 2007; PATTIARATCHI and WIJERATNE, 2009), including several

tide gauges in the South Atlantic where tsunamis had not been previously reported (WOODWORTH *et al.*, 2005; DRAGANI *et al.*, 2006; FRANÇA and DE MESQUITA, 2007; CANDELLA *et al.*, 2008). The tsunami was also recorded in far distant regions of the North Pacific and North Atlantic (RABINOVICH *et al.*, 2006; THOMSON *et al.*, 2007). The large volume of observational data associated with this event, combined with the extensive spatial distribution of the observations, has enabled us to revise some established concepts regarding tsunami propagation and the evolution of tsunami energy with time and distance from the source region.

Based on data from the 1960 Chilean tsunami (c.f. MILLER *et al.*, 1962), MUNK (1963) suggested that tsunami energy in the ocean decays much like sound intensity in an enclosed room. VAN DORN (1984) used this “acoustic analog” to examine the decay of a few major tsunami events in the Pacific Ocean. Data from these events led him to conclude that, after an initial 40-h “diffusion period” (the time for tsunami waves to become isotropically distributed),  $t_d$ , the energy for all trans-Pacific tsunamis decays in a uniformly exponential manner with the form

$$E(t) = E_0(t)e^{-\delta t}, \quad t > t_d, \quad (1)$$

where  $E_0$  is the tsunami energy index,  $\delta$  is the energy decay (attenuation) coefficient and  $t_0 = \delta^{-1}$  is the *e*-folding “decay time”, which was estimated to be nearly uniform at  $t_0 \approx 22$  h. Similar estimates for the Indian and Atlantic oceans (VAN DORN, 1987), based on the few available records for the 1960 Chilean tsunami, yielded smaller decay times of 14.6 and 13.3 h, respectively. Both MUNK (1963) and VAN DORN (1984, 1987) postulated that the main energy losses are associated with absorption during multiple reflections from the mainland coasts at a rate of about  $e^{-1}$  per reflection. Thus, the decay time for each

<sup>1</sup> Department of Fisheries and Oceans, Institute of Ocean Sciences, 9860 West Saanich Road, Sidney, BC V8L 4B2, Canada. E-mail: Alexander.Rabinovich@dfo-mpo.gc.ca; A.B.Rabinovich@gmail.com; Richard.Thomson@dfo-mpo.gc.ca

<sup>2</sup> Russian Academy of Sciences, P.P. Shirshov Institute of Oceanology, 36 Nakhimovsky Pr, Moscow 117997, Russia.

<sup>3</sup> Instituto de Estudos do Mar Almirante Paulo Moreira, 253 Rua Kioto, Arraial do Cabo, RJ 28930-000, Brazil. E-mail: RCandella@gmail.com

ocean was assumed to be of the order of the mean “reflection” time defined as

$$t_r = L^*/c, \quad (2)$$

where  $c = \sqrt{gH}$  is the long-wave speed in midocean,  $g$  is the gravitational acceleration,  $H$  is the mean ocean depth, and  $L^*$  is the mean-free travel path of tsunami waves. It follows from this formulation that the smaller  $L^*$  values for enclosed and semi-enclosed seas should lead to smaller decay times. In particular, for three records of the 1983 tsunami in the Sea of Japan, VAN DORN (1987) estimated a uniform decay time of 8.6 h. However, SATAKE and SHIMAZAKI (1988), who used low-pass filtered data for two tsunamis in the Sea of Japan (1964 and 1983), obtained much larger values of  $t_0 \approx 22.5$  h. Although the larger values were likely due to filtering, results for each event were consistent among the sites investigated. In contrast, OH and RABINOVICH (1994) found significantly different  $t_0$  values for various coastal sites for the 1993 tsunami in the Sea of Japan, with decay times ranging from 3.1 h for the open-sea island station Ulleungdo to 13.3 h for the mainland station Pohang (Korea). According to the authors, the large differences in  $t_0$  demonstrate that the rate of tsunami energy decay for a given event varies spatially. The authors assumed that this rate is dependent on the quality factor ( $Q$ -factor) of a particular location rather than on the source characteristics or the  $Q$ -factor of the sea as a whole.

Understanding how tsunamis evolve and decay over time and space are of primary importance both for tsunami science and for tsunami warning and mitigation. In the studies mentioned previously, this understanding has been limited by the small number, low spatial density, and relatively low quality (digitized analog records from coastal tide gauges) of the available tsunami records. The extensive data collected during the global 2004 Sumatra tsunami enable us to return to this major problem and to compare near-field and distal energy characteristics of tsunami waves collected from both island and mainland stations throughout the World Ocean. Moreover, we have been able to supplement our study using estimates extracted from four precise deep-ocean bottom pressure stations in the northeast Pacific (RABINOVICH *et al.*, 2011); i.e., stations which are free from

distortion by topographic effects and therefore enable us to examine “pure energy decay” in the open ocean.

## 2. Observations

The 2004 Sumatra tsunami was recorded by roughly 250 stations in the Global Ocean. The data were heterogeneous in that the quality of the records, the wave height resolution, the sampling interval and other characteristics were significantly different among the various tide gauges. In fact, the most laborious part of the analysis of tsunami records is the careful examination, verification, and correction of the observational data and the extraction of tsunami signals from these data (c.f. GORING, 2008). We mainly worked with the raw data and found that most of the time series had one or more problems, including gaps, “spikes”, time shifts, data offsets, or poor resolution. In previous studies we conducted on the 2004 tsunami waves recorded in the Indian (RABINOVICH and THOMSON, 2007), South Atlantic (CANDELLA *et al.*, 2008), North Atlantic (RABINOVICH *et al.*, 2006; THOMSON *et al.*, 2007) and North Pacific (RABINOVICH *et al.*, 2006) oceans, we fixed problems with many of the tsunami records in the various regions. However, for the present study, we have incorporated many more stations (in particular, those located in the southern and tropical parts of the Pacific Ocean, including the coasts of South America, New Zealand and Australia) so we had to thoroughly check all new data, verify them, and then correct any errors. Several records could not be analyzed because they had too many gaps or were collected by faulty instruments.

It is also important to emphasize that data which we found suitable for determining statistical characteristics were not necessarily adequate for examining energy decay. A serious inadequacy was the long (15–60 min) sampling interval at some tide gauges. Although the tsunami signal was evident in these records, these records were of little use for decay-time analyses. As a consequence, we excluded all records having a sampling interval longer than 15 min and retained only a limited number of records with a sampling interval of 15 min (those with a

strong and clear tsunami signal and low noise level). An additional problem was the short length of some of the available records. For many tsunami research studies, record length is not a critical factor; for the examination of energy decay it is. For distant records, we found that the tsunami energy decays quite slowly, which means that tsunami records of several days are needed to correctly estimate the decay time. Several high quality tsunami records had to be excluded from the energy decay analysis because the records were too short.<sup>1</sup>

The most serious problem is the signal-to-noise (S/N) ratio; i.e., the ratio of recorded tsunami wave amplitudes to the background oscillation amplitudes. Our ability to detect tsunami waves in tide gauge records and to estimate parameters for these waves, including the decay time, strongly depends on this ratio. For the 2004 Sumatra tsunami in the Indian Ocean records, the S/N ratio ranged from 40:1 to 20:1, so that the detection and estimation of tsunami parameters was straightforward (c.f. RABINOVICH and THOMSON, 2007). However, for the North Pacific and North Atlantic records, the S/N ratio ranged from 4:1 to 1:1, or even lower at some sites, making tsunami detection and analysis difficult (RABINOVICH *et al.*, 2006; THOMSON *et al.*, 2007). Low signal-to-noise ratios were also found for stations located on the northern and eastern coasts of Australia, the northern coast of New Zealand, southern coast of Chile, and several other coastal regions.

There are several factors that cause high background noise level and difficulties in tsunami detection: (1) The nonlinear interaction between wind waves and swell, especially in stormy weather, generates infragravity (IG) waves (c.f. HOLMAN *et al.*, 1978; BATTJES, 1988; RABINOVICH, 2009). Typical IG wave periods range from 30 to 300 s, although during storm conditions these waves can have periods of up to 35–40 min (KOVALEV *et al.*, 1991). At exposed coastal sites (in particular, those situated on the coast of New Zealand and at several sites on the coasts of California and Alaska), IG waves produce significant background noise at tsunami frequencies, creating

serious problems in identifying weak tsunamis (RABINOVICH and STEPHENSON, 2004); (2) partially enclosed basins, such as bays, harbours, and fjords are usually well protected from wind waves and swell but have natural (eigen) oscillations (“harbour oscillations” or “harbour seiches”) that exist almost permanently (c.f. NAKANO and UNOKI, 1962; WILSON, 1972; RABINOVICH, 2009). Incoming tsunami waves do not normally generate separate oscillations with different (additional) periods but simply amplify existing seiches. Quite often this amplification is not abrupt but gradual, making it difficult to define the exact arrival time and to separate seismically generated tsunami waves from common atmospherically generated seiches; and (3) atmospheric disturbances occasionally may generate pronounced longwave oscillations that have the same temporal and spatial scales as tsunami waves and sometimes even affect coasts in a similarly destructive way. These waves are known as *meteorological tsunamis* (c.f. RABINOVICH, 2009). One such event, with strong tsunami-like oscillations, was forced by an intense cyclone travelling along the east coasts of the United States and Canada roughly 0–48 h before the arrival of the 2004 Sumatra tsunami at these coasts. It was difficult to distinguish the tsunami waves from the storm-induced meteorological tsunami-like waves (THOMSON *et al.*, 2007).

One of the main reasons for conducting a preliminary analysis of tide gauge data (de-tiding, low-pass and high-pass filtering), is to diminish the background noise level and thereby improve the signal-to-noise ratio. However, despite this preliminary analysis, significant numbers of records, especially those for far-field regions where the tsunami signal was relatively weak, could still not be included in our examination of tsunami energy decay. In particular, of the 32 tide gauges in the northwestern Atlantic that recorded the 2004 tsunami signal (THOMSON *et al.*, 2007), only five, specifically Charlotte Amalie (US Virgin Islands), Magueyes (Puerto Rico), Bermuda, Trident Pier (Florida) and Atlantic City (New Jersey), were found to be appropriate for the present study (see Fig. 1 for site locations). The situation for the northeast Pacific was a little better because there were no storm passing through the region at the time of the event; of the 25 tsunami

<sup>1</sup> Unfortunately, there was little effort to continue records longer than 1–2 days after the first tsunami arrival; in future, this problem should be taken into account.

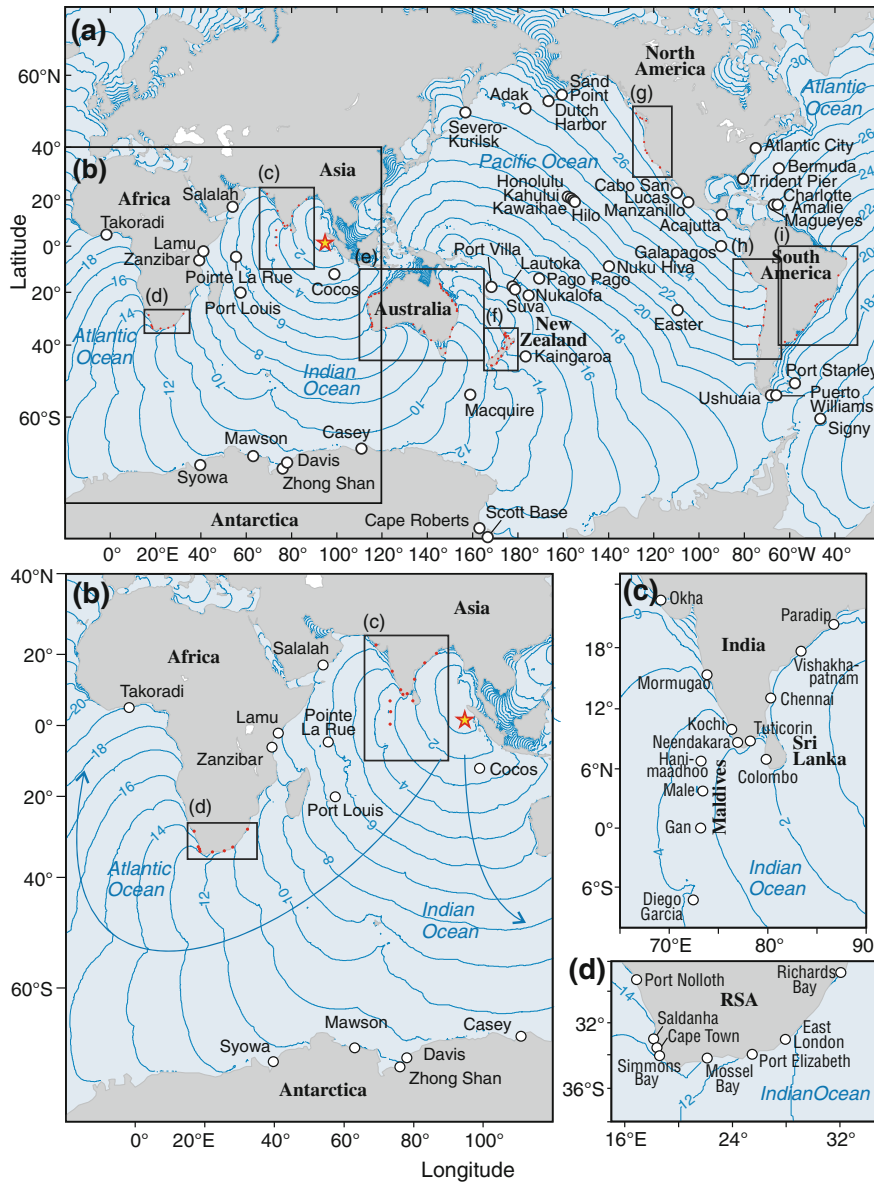


Figure 1

Maps of the Indian, Atlantic and Pacific oceans showing the location of the  $M_w = 9.3$  Sumatra earthquake epicenter (*star*) and positions of tide gauges (*circles*). **a** Map of the entire World Ocean with boxes labelled **(b-i)** denoting eight oceanic regions detailed in separate maps; **b** map of the Indian Ocean; *curved blue arrows* indicate directions of “western” and “eastern” branches of the propagating tsunami energy flux; **c** map of India and the Maldives with positions of tide gauges; **d** as with **c** but for the Republic of South Africa; **e** as with **c** but for Australia; the *two boxes* indicate regions shown in separate maps “I” and “II”; **f** as with **c** but for New Zealand; **g** as with **c** but for the Pacific coast of North America; *empty squares* indicate positions of the open-ocean DART stations 46405 and NeMO and ODP CORK station 1301. **h** and **i** are the same as **c** but for the Pacific and Atlantic coasts of South America, respectively. *Solid thin blue lines* are hourly computed isochrones of the tsunami travel time from the source area

records available (RABINOVICH *et al.*, 2006), 13 with relatively high S/N ratio were selected for our analysis (Fig. 1a, g). A similar selection procedure was undertaken for other regions.

Altogether, we identified 173 tsunami records that were suitable for examining the 2004 tsunami energy decay and other parameters of this tsunami (sites are shown in Fig. 1). Further analysis indicated that, for

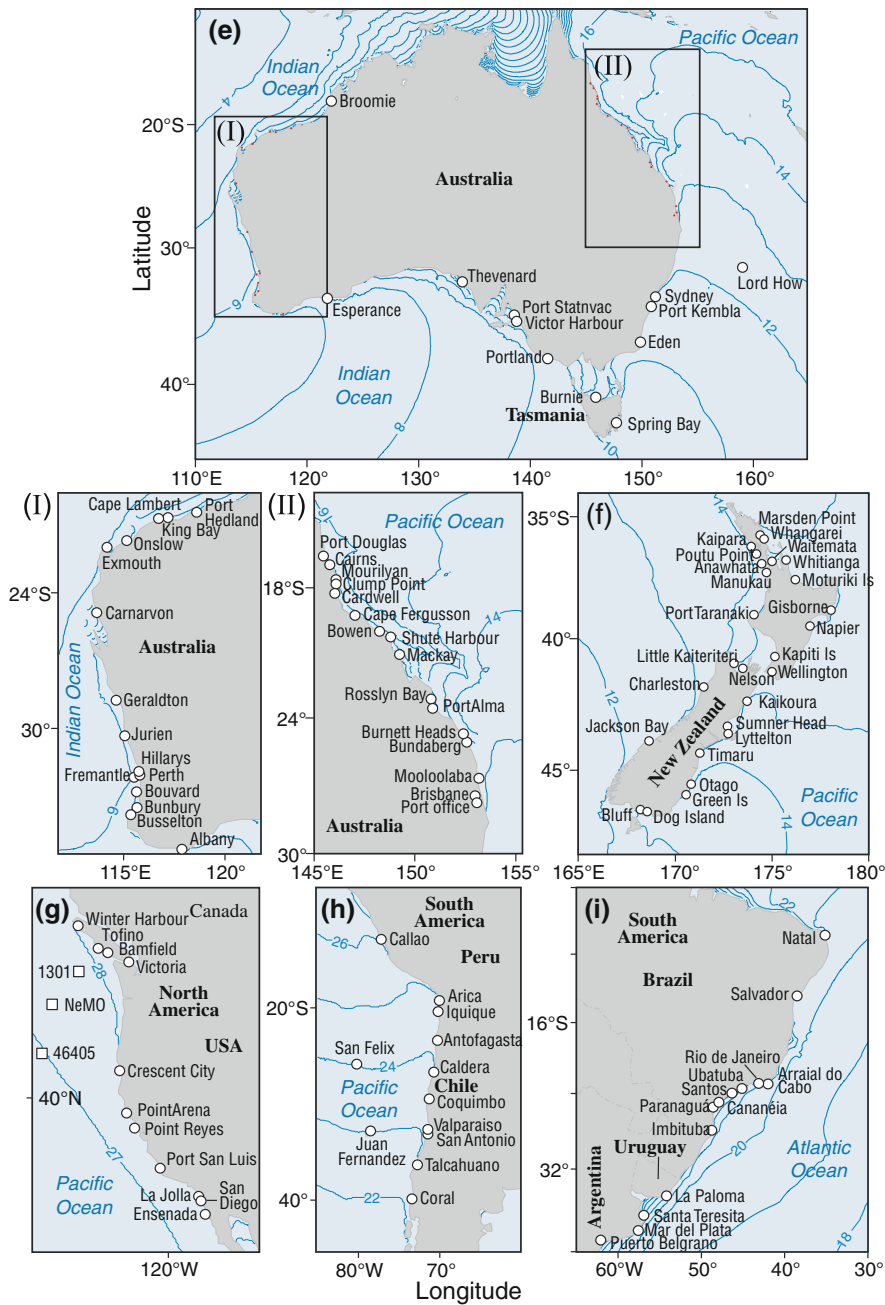


Figure 1 continued

the reasons listed above, the records for eight of these stations were not suitable for evaluating energy decay. Nevertheless, we decided to include these stations in the corresponding tables because some other tsunami parameters estimated from these

records could be useful for future tsunami studies of the 2004 event.

These 2004 tsunami data came from a great number of sources. In our previous studies of the event, we used some of these data and described the



respective data sources. The list of these previously analyzed data, the number of records in specific regions<sup>2</sup> and the references are:

1. Indian Ocean, including the Republic of South Africa (RSA), and Australian Antarctic stations: 33 stations (Fig. 1a–d) (RABINOVICH and THOMSON, 2007);
2. South Atlantic: 18 stations (Fig. 1a, i) (CANDELLA *et al.*, 2008);
3. North Atlantic: five stations (Fig. 1a) (RABINOVICH *et al.*, 2006; THOMSON *et al.*, 2007);
4. North Pacific: 17 stations (Fig. 1a, g) (RABINOVICH *et al.*, 2006).

There are a total of 73 “old” records. It should be noted that, in general, the Indian Ocean records (1) are well known and have been actively examined to estimate parameters of the observed tsunami waves (c.f. MERRIFIELD *et al.*, 2005; ABE, 2006; NAGARAJAN *et al.*, 2006; LEONARD, 2006). They also have been extensively used to reconstruct the source of the 2004 tsunami (LAY *et al.*, 2005; FINE *et al.*, 2005; TANIOKA *et al.*, 2006; FUJII and SATAKE, 2007). The South Atlantic tsunami records (2) have also been analyzed by other authors (c.f. WOODWORTH *et al.*, 2005; DRAGANI *et al.*, 2006; FRANÇA, and DE MESQUITA, 2007). However, there have been no attempts to estimate the 2004 tsunami energy decay from these data.

The remaining 100 records are mainly located in the southern and tropical parts of the Pacific Ocean and on the coast of Australia. In contrast to the Indian Ocean data, these data have never been extensively analyzed. Only a few papers have taken some of these records into consideration (c.f. PATTIARATCHI and WIJERATNE, 2009); most information about these data and some preliminary results of their analysis can be found in reports and on websites. We have used the following data:

5. Australia, including Macquarie and Lord Howe islands: 45 stations (Fig. 1a, e with two additional insets: “I” and “II”).

The data are from three main sources: (a) the Australian Bureau of Meteorology (<http://www.bom.gov.au/oceanography>); (b) the Department of Transport—Government of Western Australia (<http://www.dpi.wa.gov.au/imarine/19383.asp>); and (c) the Department of Environment and Resource Management, Queensland Government, Maritime Safety Queensland (<http://www.derm.qld.gov.au/register/p01500aa.pdf>). The 2004 tsunami records for the coast of Australia allow detailed analysis of the tsunami evolution along this coast.

6. New Zealand (NZ), including Kaingaroa (Chatam Island): 27 stations (Fig. 1a, f).

The data were provided by the National Institute of Water and Atmospheric Research (NIWA) (<http://www.niwa.co.nz/our-science/coasts/research-projects/all/physical-hazards-affecting-coastal-margins-and-the-continental-shelf/news/sumatra>) and by Mulgor Consulting Ltd. (<http://www.mulgor.co.nz/SumatraTsunami/index.htm>). Thus, for this relatively small region there were numerous records, enabling us to examine the influence of local topographic features on the tsunami behaviour.

7. NZ Antarctic: Two stations. Unique records from two stations located near and on the Ross Ice Shelf as far south as 77–78°S, about 10,000 km from the source area (Fig. 1a).

Obtained from NIWA and Mulgor Consulting Ltd.

8. Pacific coast of South America, including Juan Fernández, San Felix, Easter (Pascua) and Galapagos islands: 14 stations (Fig. 1a, h)

Data were obtained from the Servicio Hidrográfico y Oceanográfico (SHOA), Arma de Chile, and from the Pacific Tsunami Warning Center (Honolulu, HI).

9. Tropical Pacific, including the Hawaiian Islands: ten stations (Fig. 1a).

The data were obtained from the Australian Bureau of Meteorology, the Pacific Tsunami Warning Center (Honolulu, HI) and the West Coast/Alaska Tsunami Warning Center (Palmer, AK).

10. Records from Ensenada (Mexico) and Puerto Williams, Tierra del Fuego (Chile) (Fig. 1a),

<sup>2</sup> These numbers include only those records selected for the present study; the actual number of records described in these publications is much higher but many of the records were deemed not appropriate for examination of the energy decay for the reasons mentioned above.

obtained from CICESE (Ensenada, Mexico) and SHOA (Chile), respectively.

In general, it is fair to state that, despite the problems previously described, we were able to collect a large amount of high-quality observational data enabling us to investigate the global-scale properties of the 2004 tsunami. The data are related to three distinct ocean basins (Indian, Atlantic and Pacific) separated by a wide range of different distances from the source area. The specific locations of tide gauges were also quite different: some were situated on isolated islands in the open ocean, others on exposed mainland coasts or, in contrast, in deep inlets, bays and harbours. Clearly, regional and local topographic features significantly influence the observed tsunami waves. However, taken together, these numerous records selected for this study provide good statistics and possibilities for an extensive analysis of tsunamis waves.

The main focus of the present study is the energy decay of the tsunami waves observed during the 2004 event. Because of their scientific interest and importance, other parameters of the waves estimated during determination of the decay times, such as arrival time and maximum wave height, are also provided. These parameters were also found to be correlated with the energy decay parameters. For this reason, we have tabulated and described the major tsunami parameters. Focus is on the records from groups (5–10) listed above which were not examined in our previous studies.

### 3. Analysis

The available tide gauge records had markedly different durations, sampling intervals and quality, and they came from considerably different types of instruments (some of them were digitized records from archaic pen-and-paper analog tide gauges). Despite these constraints, we tried to be consistent in our analysis by keeping the analysis format and by assembling stations into comparable groups. At the same time, we tried to adapt our analysis to the data, taking into account the wave properties at each site (tidal range, intensity of high-frequency and low-frequency oscillations, and length of tsunami “ringing”). The main

purpose of the preliminary analysis was to improve the S/N ratio and to isolate the actual tsunami signal from the background oscillations. The corrected and verified records were analyzed as follows:

1. *De-tiding* Except for a few NZ residual series, all records we examined were original records that included the tides. Tides, which were quite high at most stations, were estimated using a least squares method of harmonic analysis and then subtracted from the original series. The residual (de-tided) time series were used in all subsequent analyses.
2. *Low-frequency filtering* was used to suppress intense high-frequency noise mainly associated with IG-waves generated by the nonlinear interaction of wind waves and swell. This was a serious problem for exposed coastal sites, in particular those located along the coasts of New Zealand (NZ) and also for some sites on the West Coast of the USA (e.g., Point Reyes and Arena Cove) and Australia. The de-tided records at these sites were low-pass filtered with 6- or 20-min Kaiser-Bessel windows (c.f. EMERY and THOMSON, 2003), with the choice of filter length for some of the NZ sites dependent upon the noise level. Tide gauges located at sheltered sites did not experience IG-waves and were not filtered.
3. *High-frequency filtering* was used to remove sea level variations associated with synoptic atmospheric activity. These variations in the residual sea level records were removed using a high-pass 4-h Kaiser-Bessel filter that isolates the tsunami frequency, thus simplifying tsunami detection and examination.

Statistical analysis of the residual and filtered series provided estimates of the basic characteristics of the tsunami waves (in particular, arrival time, travel time and maximum trough-to-crest wave height).<sup>3</sup> Additionally, we applied time–frequency (wavelet-type) analysis to investigate time–frequency variations of the tsunami waves and to help identify

<sup>3</sup> Filtering helps us to identify tsunami waves and to isolate them; at the same time it diminishes the actual wave heights and distorts the arrival waveforms (EMERY and THOMSON, 2003; CANDELLA et al., 2008). To avoid such errors, we analyzed the filtered series in combination with the residual (de-tided) series.

the tsunami arrival times (see RABINOVICH *et al.*, 2006; RABINOVICH and THOMSON, 2007 for details).

As illustrated by the examples in Fig. 2 for three island and three mainland stations, the tsunami energy followed an exponential-type decay with time, with the decay at island tide gauge sites typically more rapid than at mainland sites. This basic decay is superimposed on periodic “bursts” of energy that likely arise from tsunami reflection at continental boundaries. To investigate the evolution of tsunami energy with time, we estimated the tsunami variance for 12- and 6-h data segments. Specifically, these

variance values were used to estimate parameters of the tsunami energy decay: the tsunami energy index ( $E_0$ ), the decay (attenuation) coefficient ( $\delta$ ), and the decay time ( $t_0$ ). We applied a least squares procedure to estimate  $E_0$  and  $\delta$  ( $t_0$ ) for various stations. We could not identify the exact diffusion periods,  $t_d$ , (the time for tsunami waves to become isotropic) because these times were difficult to define precisely, in part because the waves never actually become “isotropically distributed”. Instead, we began our calculations from the time  $t = t_m$  of the maximum observed variance which, for some stations located near the

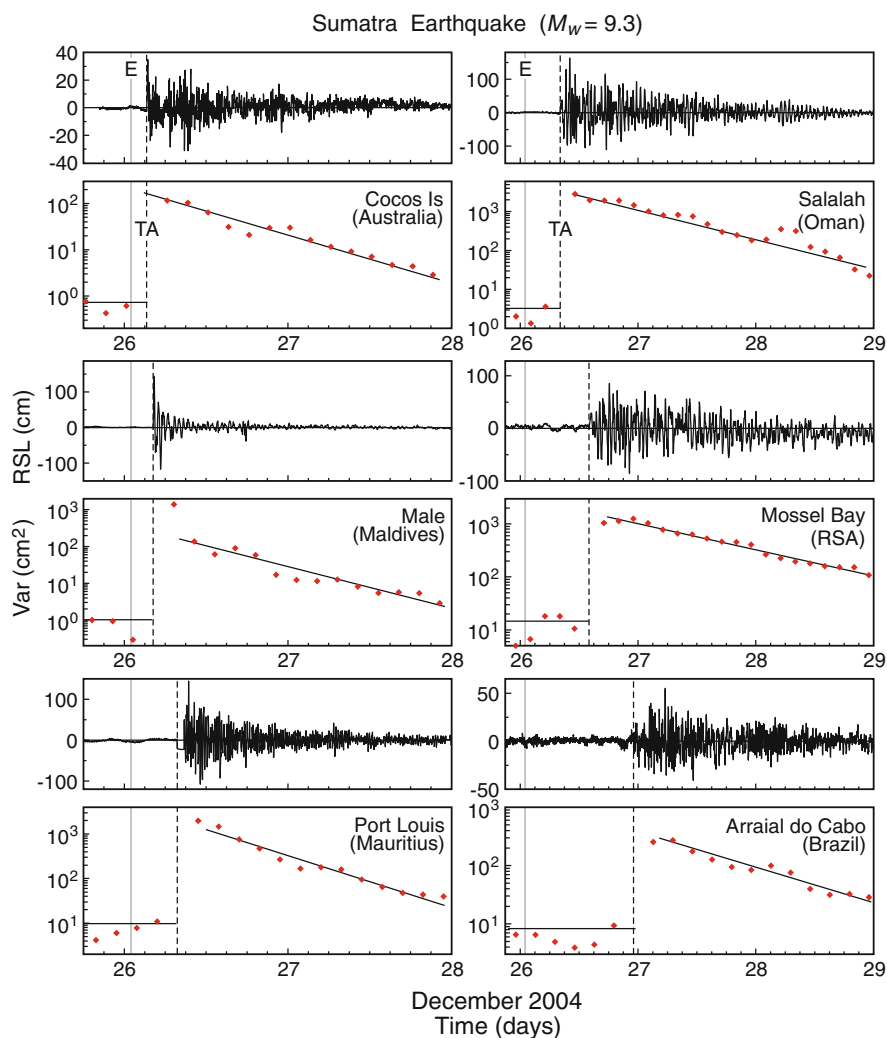


Figure 2

De-tided, low-pass filtered tsunami records for six selected sites for the 2004 Sumatra tsunami and associated record variances. *Solid vertical lines* labelled “E” denotes the time of the main earthquake shock, while *dashed lines* labelled “TA” indicate the tsunami arrival time. *Solid lines* are least squares fits to the variance decays



source region, almost coincided with the arrival time of the first wave peak or trough (Fig. 2). Confidence levels for  $E_0$  and  $\delta$  were calculated in the same manner as for linear regression estimations (c.f. EMERY and THOMSON, 2003). Because the decay times,  $t_0$ , are estimated from  $\delta$ , the confidence levels for  $t_0$  can be estimated from the confidence levels for  $\delta$ . All calculations were performed in two ways: with 12-h segments and 6-h overlap (i.e. with variance values every 6 h) and with 6-h segments and 3-h overlap (with variances every 3 h). In general, the results are similar.

The tsunami energy index ( $E_0$ ) is a measure of the observed tsunami energy for a specific site. From this point of view, this is a useful characteristic which can be compared with the results of numerical modelling. The problem, however, is that for various tide gauges we have widely different sampling intervals ranging from 0.5 to 15 min. It is obvious that long sampling intervals can lead to a marked distortion of the wave properties (c.f. LEONARD, 2006). Waves are not properly represented by the digital records if the sampling interval is of long duration relative to the actual wave period. The resulting aliasing can significantly affect the statistical results, especially maximum wave heights (EMERY and THOMSON, 2003; CANDELLA *et al.*, 2008) and energy characteristics. The influence of the actual sampling interval on recorded tsunami wave parameters depends on two primary factors: (1) the frequency and energy content of the arriving waves, and (2) the frequency response of the observational site. The first is known to be fairly uniform for each event throughout the entire World Ocean, while the second depends on the local topographic response function (c.f. RABINOVICH and STEPHENSON, 2004).

CANDELLA *et al.* (2008) attempted to account for the attenuation of the maximum tsunami wave heights for the 2004 tsunami as a function of the instrument sampling intervals. For this purpose, they selected several stations with short samplings and relatively strong tsunami signals and artificially averaged and then resampled these records with larger intervals (2, 3, ..., 15 min). The resampled series were then used to determine the corresponding statistical parameters for the tsunami waves. We used a similar approach to estimate the attenuation factors

(coefficients)  $R_{E_0}^k(j)$  for the tsunami energy index  $E_0^k(j)$  for  $k$ -th station and sampling interval  $j$  (in min). The records from five representative World Ocean stations were used for this purpose (Fig. 1): four of these stations (Cocos, Hillarys, Arraial do Cabo and Crescent City) had 1-min sampling and one (Syowa, Japanese Antarctic) had 30-s sampling; the latter was averaged and resampled to 1 min. The attenuation factors were estimated through the ratio:

$$R_{E_0}^k(j) = E_0^k(j)/E_0^k(1) \quad (3)$$

measured with respect to the observed tsunami energy index  $E_0^k(1)$  for the records with 1-min sampling. Calculated factors  $R_{E_0}^k(j)$  for individual stations are shown in Fig. 3a and in Table 1. Although results differ slightly from one site to another, there is a general consistency among the estimates. More specifically, the longer the sampling interval, the greater

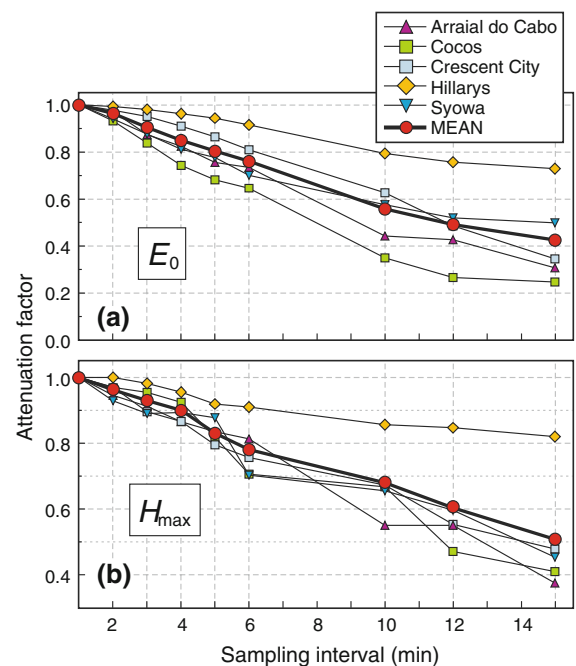


Figure 3

**a** Attenuation factor (coefficient)  $R_{E_0}^k(j)$  for the tsunami energy index  $E_0^k(j)$  for  $k$ -th station and sampling intervals  $j = 1, 2, 3, 4, 5, 6, 10, 12$  and  $15$  min at five selected stations. Also shown is the mean attenuation coefficient  $R_{E_0}(j)$  averaged over five stations; **b** as in **a** but for the attenuation coefficient  $R_{max}^k(j)$  for the maximum wave height for the  $k$ -th station and  $R_{max}(j)$  for the mean value. Results demonstrate the effect of sampling time interval on the estimated tsunami parameters

the attenuation of the recorded energy indices. The individual factors were subsequently used to calculate mean attenuation coefficients:

$$R_{E_0}(j) = \frac{1}{n} \sum_{k=1}^n R_{E_0}^k(j), \quad (4)$$

where for this study  $n = 5$ . According to these estimates, the energy index for the 2004 tsunami is attenuated by  $\sim 20\%$  for records with 5-min sampling and by almost 60% for records with 15-min sampling (Table 1).

For comparison, we obtained similar estimates based on the same stations for maximum wave heights and estimated the corresponding attenuation factor,  $R_{\max}^k(j)$ , for each  $k$ -th station as well as the mean attenuation coefficient  $R_{\max}(j)$ . The results are listed in Table 2 and plotted in Fig. 3b. Maximum wave heights diminish by approximately 17 and 50% for sampling intervals of 5 and 15 min, respectively.

It is clear from Fig. 3 that the attenuation factors for individual stations can be significantly different from the mean attenuation factors,  $R_{E_0}(j)$  and  $R_{\max}$

( $j$ ), derived from this set of stations; however, in general, these estimates enable us to partially account for the influence of sampling intervals on the observed statistical parameters of tsunami waves.

#### 4. Results

Our findings reveal that the 2004 Sumatra tsunami was recorded throughout the entire World Ocean. Global tsunami propagation models (Trov *et al.*, 2005; KOWALIK *et al.*, 2007) demonstrated that mid-ocean ridges served as wave-guides for the 2004 tsunami waves, efficiently transmitting tsunami energy from the source area in the Indian Ocean to far-field regions in the Pacific and Atlantic oceans. The tsunami energy was spread over a wide area by two main branches. One branch (the “western” or “Atlantic” branch) extended mainly westward and southwestward across the Indian Ocean, around Africa into the Atlantic Ocean, and then northward along the Mid-Atlantic Ridge into the North Atlantic (Figs. 1, 4). The

Table 1  
Tsunami energy index  $E_0$  ( $\text{cm}^2$ ) obtained for selected re-sampling interval ( $j$ )

Station	Country	Sampling interval, $j$ (min)								
		1	2	3	4	5	6	10	12	15
Cocos Is.	Australia	1.00	0.93	0.84	0.74	0.68	0.64	0.35	0.26	0.24
Hillarys	Australia	1.00	0.99	0.98	0.96	0.94	0.91	0.79	0.76	0.73
Arraial do Cabo	Brazil	1.00	0.97	0.87	0.82	0.75	0.73	0.44	0.42	0.31
Crescent City	USA	1.00	0.98	0.95	0.91	0.86	0.81	0.62	0.48	0.34
Syowa, Antarctica	Japan	1.00	0.94	0.87	0.81	0.78	0.70	0.57	0.52	0.50
Mean attenuation factor ( $R_{E_0}$ )	–	1.00	0.96	0.90	0.85	0.80	0.76	0.56	0.49	0.42

The last row is the mean attenuation coefficient  $R_{E_0}(j)$  defined by Eq. 4

Table 2  
Maximum trough-to-crest wave height,  $H_{\max}$  (cm), obtained for selected re-sampling interval ( $j$ )

Station	Country	Sampling interval, $j$ (min)								
		1	2	3	4	5	6	10	12	15
Cocos Is.	Australia	1.00	0.97	0.95	0.92	0.82	0.70	0.67	0.47	0.41
Hillarys	Australia	1.00	1.00	0.98	0.96	0.92	0.91	0.86	0.85	0.82
Arraial do Cabo	Brazil	1.00	0.95	0.91	0.86	0.84	0.81	0.55	0.55	0.37
Crescent City	USA	1.00	0.97	0.90	0.87	0.79	0.76	0.67	0.55	0.48
Syowa, Antarctica	Japan	1.00	0.93	0.89	0.88	0.79	0.70	0.65	0.60	0.45
Mean attenuation factor ( $R_{\max}$ )	–	1.00	0.96	0.93	0.90	0.83	0.78	0.68	0.60	0.51

The last row is the mean attenuation coefficient  $R_{\max}(j)$

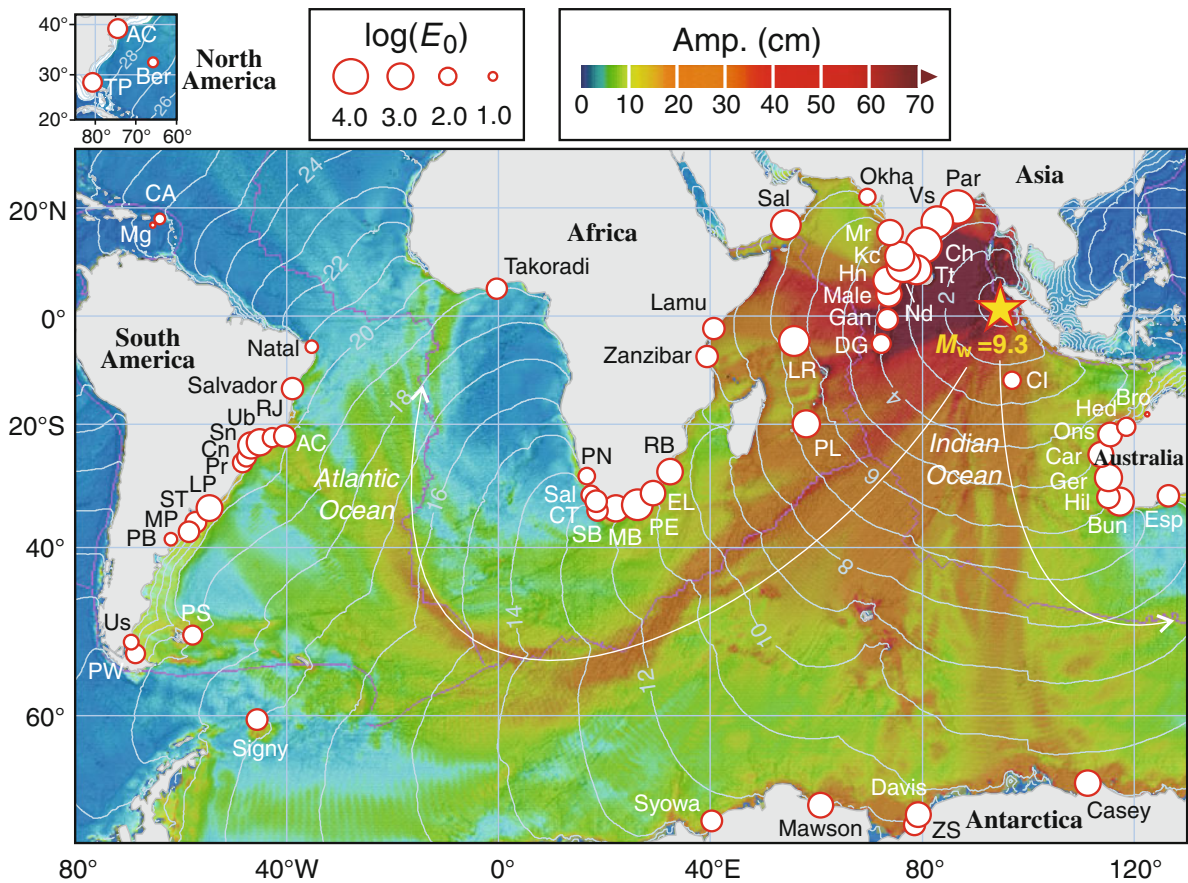


Figure 4

Simulated tsunami wave heights from Trtov *et al.* (2005) along with the tsunami wave energy index,  $E_0$ , calculated for the Indian and South Atlantic oceans. The *small inset* above the main plot shows locations of three North Atlantic stations: Trident Pier, Atlantic City (both on the coast of North America) and the Bermuda Islands. *Solid thin grey lines* are hourly isochrones of the tsunami travel time from the source area. *Yellow star* indicates the 2004 Sumatra earthquake epicenter. *Curved white arrows* indicate directions of “western” and “eastern” branches of the propagating tsunami energy flux

second major branch (the “eastern” or “Pacific” branch) extended southward and southeastward around Australia into the Pacific Ocean, northeastward around New Zealand, then along the coasts of South and North America to the northernmost parts of the Pacific (Fig. 5). About 30% more tsunami energy entered the Atlantic Ocean through the western branch than went into the Pacific Ocean via the eastern branch (KOWALIK *et al.*, 2007). This energy distribution was mainly related to the orientation of the earthquake rupture. In general, there is good agreement between simulated (Trtov *et al.*, 2005) and measured maximum waves as indicated by the marked coincidence between computed “branches” of energy flux and zones of high recorded wave height (c.f., Figs. 4, 5).

#### 4.1. Western Stations

There is considerable difference in the frequency of tsunami occurrence in the Indian, Atlantic, and Pacific oceans. According to GUSIAKOV (2009), about 60% of all known tsunamis have occurred in the Pacific Ocean, while only 12% have occurred in the Atlantic Ocean (mainly, in the Caribbean region) and 6% in the Indian Ocean. Historically, the Atlantic and Indian oceans have had no Tsunami Warning Systems and no standard instruments designed for tsunami measurement. The primary purpose of tide gauges in these two oceans was the measurement of relatively low-frequency processes such as tides, storm surges, seasonal and climatic sea level



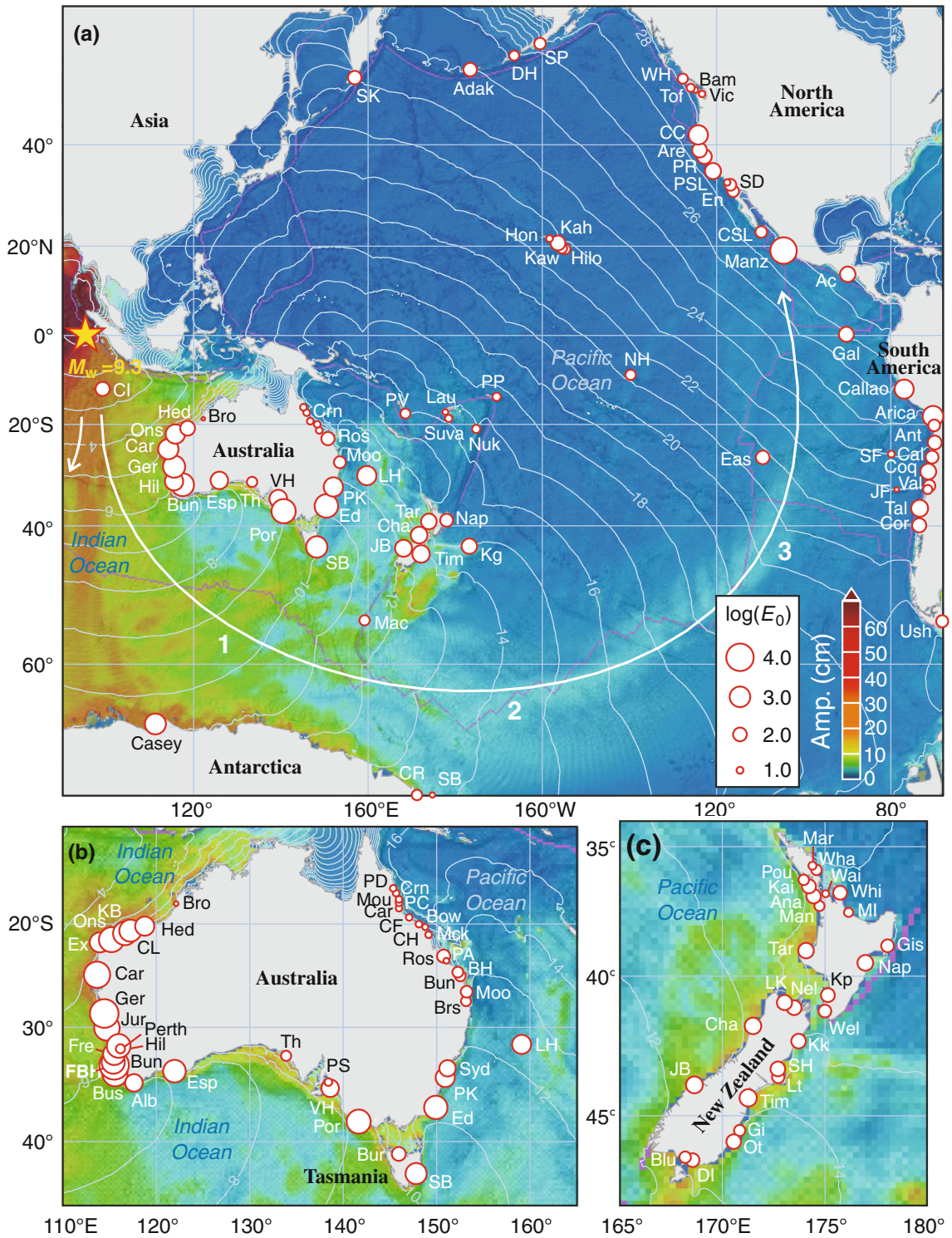


Figure 5

The same as in Fig. 4 but for the Pacific Ocean: **a** entire Pacific Ocean; **b** Australia; and **c** New Zealand. In **a**, the curved white arrow shows the direction of the “eastern” branch of the propagating tsunami energy, while labels 1–3 indicate the Southeast Indian Ridge (“1”), Pacific Antarctic Ridge (“2”), and East Pacific Rise (“3”)

variations, and long-term trends (c.f. WOODWORTH *et al.*, 2005). The tsunami records associated with the 2004 event represent the first high quality tsunami records in the Atlantic and Indian oceans.<sup>4</sup>

The principal tsunami parameters estimated for the “western” group of stations are presented in Tables 3 and 4. Specifically, we tabulated the following parameters: (1) The arrival time (UTC) of the first wave, (2) the travel time of the first wave, (3) the maximum trough-to-crest (or crest-to-trough) wave height, (4) the observed time (UTC) of the maximum wave, (5) the energy index  $E_0$  and (6) the energy  $e$ -folding decay time,  $t_0$ , plus confidence levels. Some of these parameters presented in our earlier studies (RABINOVICH and THOMSON, 2007; CANDELLA *et al.*, 2008) have been carefully re-examined here. The energy circles (proportional to  $\log E_0$ ) in Figs. 4 and 5 have been adjusted for the effect of gauge sampling interval. However, maximum wave heights and energy indices in Tables 3 and 4 have not been corrected for sampling interval; this correction can be approximated by dividing the tabulated values by the corresponding mean attenuation coefficients from Tables 1 and 2.<sup>5</sup>

Figure 4 shows a major branch of the tsunami energy directed into the Atlantic Ocean with energy flux propagating mainly along mid-ocean ridges. The observed values of  $E_0$  correspond well to the results of numerical computations (TITOV *et al.*, 2005). Specifically, tsunami-exposed continental coasts received much more tsunami energy than lee coasts. For example, estimated  $E_0$  values on the exposed east and southeast coasts of India and South Africa were 1,352–7,350 and 628–3,267  $\text{cm}^2$ , respectively, while corresponding values for the protected west (leeward) coasts of these two territories were 42–2,127 and 75–254  $\text{cm}^2$ , respectively (c.f. Tables 3, 4).

The statistical parameters presented in Tables 3 and 4 are of particular interest since they can be used to verify existing numerical models and to examine

topographic effects on propagating tsunami waves. Consider the two pairs of Argentinean stations in the Atlantic Ocean which consist of stations located within a few kilometres of each other (Table 4): (1) Ushuaia 1 and Ushuaia 2; and (2) Mar del Plata 1 and Mar del Plata 2 (CANDELLA *et al.*, 2008). Records from the first pair of stations (Ushuaia) had similar statistical tsunami parameters, probably due to similarity in topographic influences (both tide gauges are located in narrow Beagle Canal in the southern part of Tierra del Fuego and are only 5 km apart). In contrast, the records and statistical parameters for the second pair of stations (Mar del Plata) were markedly different, demonstrating a pronounced influence of local topographic features; the Mar del Plata 1 tide gauge is located on a comparatively open external coast while the Mar del Plata 2 tide gauge (GLOSS<sup>6</sup> station) is situated inside a lagoon where arriving tsunami waves were strongly amplified by local resonant effects. As a result, the maximum wave height at Mar del Plata 2 was 3.5 times larger than at Mar del Plata 1.

It is logical that the maximum observed tsunami wave heights of 3–3.5 m in the Indian Ocean were observed relatively close to the source area (c.f. MERRIFIELD *et al.*, 2005; NAGARAJAN *et al.*, 2006; RABINOVICH and THOMSON, 2007), particularly on the eastern and southern coasts of India (Table 3). Maximum  $E_0$  values were also observed in this region (Fig. 4). In addition, wave heights of more than 2.5 m were recorded at Pointe La Rue (Seychelles Is.), Salalah (Oman) and Port Elizabeth (South Africa) located five to nine thousand kilometres from the source (Table 3).

In the Atlantic Ocean, maximum tsunami wave heights were measured on the southeastern coast of Brazil: 114 cm at Ubatuba and 91 cm at Arraial do Cabo.<sup>7</sup> It was along this region of the Atlantic coast of South America where the highest 2004 tsunami

<sup>6</sup> GLOSS is the Global Sea Level Observing System (<http://www.gloss-sealevel.org/>).

<sup>7</sup> An even larger maximum wave height of 123 cm was recorded at Imbituba located in the same region (MELO and ROCHA, 2005; CANDELLA *et al.*, 2008); however, this was a “pen-and-paper” analog record which was difficult to analyze. Also, CANDELLA *et al.* (2008) estimated that the actual tsunami wave height at La Paloma (Uruguay) was >1.5 m but the observed signal was strongly attenuated due to the 15-min sampling.

<sup>4</sup> CANDELLA *et al.* (2008) listed a few known historical tsunami records in the Atlantic Ocean but all of these records were relatively poor quality analog records.

<sup>5</sup> As was noted above, the sampling attenuation coefficients depend on properties of individual sites and are different for different stations; the mean coefficients give only approximate correction values.



Table 3

*Tsunami characteristics for 27 “western group” tide gauge stations located in the Indian Ocean (isolated island stations are written in italics)*

No.	Station	$\Delta t$ (min)	First wave		Maximum wave		Energy	
			Arrival time (UTC)	Travel time (h:min)	Observ. time (UTC)	Height (cm)	$E_0$ (cm <sup>2</sup> )	Decay time, $t_0$ (h)
1	Paradip (India)	6	03:27	2:28	06:42	318	3,968	13.0 ± 0.4
2	Vishakhapatnam (India)	5 <sup>a</sup>	03:35	2:36	06:25	291	2,558	13.6 ± 0.6
3	Chennai (India)	5 <sup>a</sup>	03:33	2:34	07:05	324	7,350	14.1 ± 0.8
4	Colombo (Sri Lanka)	2	03:49	2:50	(1) 06:00 <sup>b</sup> (2) 07:30 <sup>b</sup>	387 <sup>b</sup>	1,459	13.9 ± 1.0
5	Tuticorin (India)	6	04:24	3:25	04:18	181	1,352	14.7 ± 0.6
6	Neendakara (India)	15	05:08	4:09	20:15	217	2,127	20.9 ± 1.2
7	Kochi (India)	6	05:41	4:42	07:42	149	1,234	16.1 ± 0.6
8	Mormugao (India)	5 <sup>a</sup>	06:53	5:54	10:00	157	529	18.8 ± 0.7
9	Okha (India)	6 <sup>a</sup>	09:03	8:04	13:42	45	42	22.5 ± 1.7
10	<i>Hanimaadhoo (Maldives)</i>	2	04:30	3:31	04:40	217	1,127	12.8 ± 0.3
11	<i>Male (Maldives)</i>	4	04:14	3:15	04:24	215	713	14.6 ± 0.9
12	<i>Gan (Maldives)</i>	4	04:16	3:17	04:32	139	210	13.0 ± 1.2
13	<i>Diego Garcia (UK)</i>	6	04:45	3:46	04:54	90	102	13.0 ± 0.8
14	<i>Port Louis (Mauritius)</i>	2	07:46	6:47	09:26	195	1,052	13.0 ± 0.9
15	<i>Pointe La Rue (Seychelles)</i>	4	08:16	7:17	09:12	278	2,671	13.5 ± 0.7
16	Salalah (Oman)	4	08:08	7:09	10:04	278	2,335	14.5 ± 0.7
17	Lamu (Kenya)	4	09:52	8:53	10:44	100	311	13.7 ± 0.9
18	<i>Zanzibar (Tanzania)</i>	4	10:40	9:41	11:24	72	226	15.5 ± 1.1
19	Richards Bay (RSA)	3	12:06	11:07	17:45	152	850	18.3 ± 0.9
20	East London (RSA)	3	12:28	11:29	09:54 <sup>c</sup>	128	628	18.3 ± 0.6
21	Port Elizabeth (RSA)	3	13:12	12:13	22:57	268	3,267	17.0 ± 0.6
22	Mossel Bay (RSA)	3	14:01	13:02	17:51	156	1,037	20.7 ± 0.7
23	Casey (Antarctica, Austr.)	10	12:00	11:01	16:50	88	425	14.6 ± 0.7
24	Davis (Antarctica, Austr.)	10	13:10	12:11	22:20	94	346	12.8 ± 0.5
25	Zhong Shan (Antarctica, Austr.)	10	13:20	12:21	21:20	56	118	13.8 ± 0.4
26	Mawson (Antarctica, Austr.)	10	13:10	12:11	22:00	85	335	13.8 ± 0.4
27	Syowa (Antarctica, Japan)	0.5	13:40	12:41	17:30	78	199	19.5 ± 1.1

$\Delta t$  is the sampling interval for the gauge. The last column shows the mean and standard error of the decay time

<sup>a</sup> Digitized records

<sup>b</sup> The Colombo GLOSS tide gauge was severely damaged by the first tsunami waves and did not work for several hours (RABINOVICH and THOMSON, 2007). HOWEVER, PATTIARATCHI and WIJERATNE (2009) were able to use the second encoder for this gauge, together with data from an offshore S4DW wave and current recorder, to restore the missing data and evaluate maximum tsunami wave heights; for the Colombo station, the waves at 06:00 and 07:30 (UTC) had exactly the same heights

<sup>c</sup> 27th December

waves were recorded outside of the Indian Ocean. These observations refute early results by MURTY *et al.* (2005) who, based on limited data available at that time, concluded that, due to unspecified physical reasons, the 2004 tsunami waves were much smaller in the Atlantic than in the Pacific. In fact, there was a factor of 1.3 times higher flux of tsunami energy into the Atlantic Ocean than into the Pacific Ocean during the 2004 event (KOWALIK *et al.*, 2007). The smaller area of the Atlantic and the wave guide effect of the Mid-Atlantic Ridge also gave rise to intensification of

tsunami waves on Atlantic coasts (CANDELLA *et al.*, 2008). Tsunami waves from the Sumatra source area continued to propagate to the coasts of Uruguay and Brazil for approximately 21–24 h (Fig. 4). The observed tsunami arrival times were in close agreement with the Expected Time of tsunami Arrivals (ETA); tsunami travel times (relative to the main earthquake shock) are shown by the isolines (isochrones) in Figs. 1, 4 and 5.

With very few exceptions, the first recorded wave at most sites of the “western group” was positive, in

Table 4

*Tsunami characteristics for 28 “western group” tide gauge stations located in the Atlantic Ocean (isolated island stations are written in italics)*

No.	Station	$\Delta t$ (min)	First wave		Maximum wave		Energy	
			Arrival time (UTC)	Travel time (h:min)	Observ. time (UTC)	Height (cm)	$E_0$ (cm <sup>2</sup> )	Decay time, $t_0$ (h)
28	Simons Bay (RSA)	3	14:18	13:19	19:33 <sup>a</sup>	85	205	24.0 ± 1.0
29	Cape Town (RSA)	3	15:00	14:02	14:01 <sup>a</sup>	88	254	24.6 ± 1.0
30	Saldanha (RSA)	3	15:28	14:29	04:00 <sup>a</sup>	74	132	25.4 ± 2.3
31	Port Nolloth (RSA)	3	16:01	15:02	06:48 <sup>a</sup>	49	77	27.1 ± 1.6
32	<i>Signy, S. Orkney</i> (UK)	15	18:45	17:46	20:38 <sup>a</sup>	52	93	19.0 ± 2.3
33	<i>P. Stanley, Falkland Is.</i> (UK)	15	22:30	21:31	23:08	44	57	26.7 ± 3.2
34	Puerto Williams (Chile)	15	22:42	21:43	10:20 <sup>a</sup>	47	85	–
35	Ushuaia I (Argentina)	15	23:15	22:16	06:45 <sup>a</sup>	17	18	23.1 ± 3.3
36	Ushuaia 2 (Argentina)	6	23:12	22:13	13:48 <sup>a</sup>	20	18	23.4 ± 2.7
37	Puerto Belgrano (Argentina)	4 <sup>b</sup>	01:16 <sup>a</sup>	24:17	13:28 <sup>a</sup>	25	24	–
38	Mar del Plata1 (Argentina)	4 <sup>b</sup>	00:04 <sup>a</sup>	23:05	07:56 <sup>a</sup>	18	167	25.6 ± 5.4
39	Mar del Plata2 (Argentina)	6	00:09 <sup>a</sup>	23:10	06:42 <sup>a</sup>	59	166	26.9 ± 1.6
40	Santa Teresita (Argentina)	6	00:33 <sup>a</sup>	23:34	00:48 <sup>a</sup>	31	166	25.4 ± 3.2
41	La Paloma (Uruguay)	15	23:45	22:46	23:30 <sup>a</sup>	80	368	27.5 ± 1.9
42	Paranaguá (Brazil)	10 <sup>b</sup>	00:30 <sup>a</sup>	23:31	12:40 <sup>a</sup>	18	68	22.1 ± 4.7
43	Cananéia (Brazil)	2 <sup>b</sup>	00:48 <sup>a</sup>	23:49	06:38 <sup>a</sup>	31	128	19.6 ± 1.1
44	Santos (Brazil)	10 <sup>b</sup>	00:30 <sup>a</sup>	23:31	16:05 <sup>a</sup>	80	404	20.2 ± 7.5
45	Ubatuba (Brazil)	2 <sup>b</sup>	23:38	22:39	11:16 <sup>a</sup>	114	804	19.1 ± 0.9
46	Rio de Janeiro (Brazil)	10 <sup>b</sup>	23:20	22:21	07:00 <sup>a</sup>	44	61	19.4 ± 4.3
47	Arraial do Cabo (Brazil)	1	23:04	22:05	05:32 <sup>a</sup>	91	242	18.0 ± 0.7
48	Salvador (Brazil)	6	22:12	21:13	00:12 <sup>a</sup>	62	164	20.8 ± 2.0
49	Natal (Brazil)	5 <sup>b</sup>	23:09	22:10	02:07 <sup>a</sup>	17	18	21.6 ± 3.3
50	Takoradi (Ghana)	15	01:45 <sup>a</sup>	24:46	23:30 <sup>a</sup>	41	81	23.6 ± 1.2
51	<i>Bermuda</i>	6	05:06 <sup>a</sup>	28:07	11:12 <sup>a</sup>	11	7	23.3 ± 1.3
52	<i>Charlotte Amelie (VI, USA)</i>	6	05:42 <sup>a</sup>	28:43	17:30 <sup>a</sup>	16	12	24.2 ± 3.5
53	Magueyes (Puerto Rico)	6	05:54 <sup>a</sup>	28:55	17:20 <sup>a</sup>	7	2	30.8 ± 6.3
54	Trident Pier (FL, USA)	6	09:24 <sup>a</sup>	32:25	13:06 <sup>a</sup>	32	39	30.3 ± 7.6
55	Atlantic City (NJ, USA)	6	09:30 <sup>a</sup>	32:31	11: 54 <sup>a</sup>	21	41	29.2 ± 4.2

$\Delta t$  is the sampling interval for the gauge

<sup>a</sup> 27th December

<sup>b</sup> Digitized records

good agreement with the notion that the frontal wave crest from the source area propagated westward and southwestward, while the wave trough propagated in the opposite direction (c.f. TITOV *et al.*, 2005; KOWALIK *et al.*, 2007; RABINOVICH and THOMSON, 2007).

#### 4.2. Eastern Stations

Unlike the case for the Atlantic, there was no obvious “tongue” of tsunami energy directed into the Pacific Ocean (compare Figs. 4, 5). Nevertheless, the trajectory of the main “eastern” branch of energy flux

is clearly evident. After entering the Pacific Ocean from the southeastern Indian Ocean, the flux energy was directed counterclockwise around the ocean, guided by the mid-ocean ridges of the southern and eastern Pacific (specifically, the Southeast Indian Ridge, Pacific Antarctic Ridge, and East Pacific Rise, indicated in Fig. 5 by numbers “1”, “2”, and “3”, respectively). This flux transported considerable energy to the coasts of Chile, Peru, Mexico and California and was responsible for significant (>50 cm) tsunami waves recorded at several sites, in particular, at Arica, Callao, Manzanillo, Crescent City, and Port San Luis (c.f. RABINOVICH *et al.*, 2006).

Table 5

*Tsunami characteristics for 23 Australian tide gauge stations located in the Indian Ocean (isolated island stations are written in italics)*

No.	Station	$\Delta t$ (min)	First wave		Maximum wave		Energy	
			Arrival time (UTC)	Travel time (h:min)	Observ. time (UTC)	Height (cm)	$E_0$ (cm <sup>2</sup> )	Decay time, $t_0$ (h)
56	<i>Cocos Is. (WA)</i>	1	03:17	02:18	03:26	59	90	13.1 ± 0.6
57	Broomie (WA)	1	11:04 <sup>a</sup>	10:05 <sup>a</sup>	13:51	8	1	31.4 ± 22.8
58	Port Hedland (WA)	5	08:45	07:46	17:35	59	103	18.2 ± 0.9
59	Cape Lambert (WA)	5	07:55	06:56	15:50	74	215	16.1 ± 0.5
60	King Bay (WA)	5	07:50	06:51	14:00	90	317	17.8 ± 0.8
61	Onslow (WA)	5	07:25	06:26	07:35	104	441	18.3 ± 1.0
62	Exmouth (WA)	5	06:25	05:26	14:50	59	130	13.4 ± 0.7
63	Carnarvon (WA)	5	07:45	06:46	22:50	121	618	18.0 ± 1.4
64	Gerladton (WA)	5	07:30	06:31	22:45	157	1,123	17.8 ± 0.8
65	Hillarys (WA)	1	07:22	06:23	10:25	109	405	16.5 ± 1.7
66	Jurien Bay (WA)	5	07:10	06:11	20:40	85	497	17.2 ± 0.8
67	Perth (WA)	5	08:20	07:21	16:50	16	8	26.6 ± 1.9
68	Fremantle (WA)	5	07:35	06:36	22:15	92	208	19.7 ± 0.9
69	Fremantle Boat Harbour (WA)	5	07:40	06:41	05:35 <sup>b</sup>	80	231	19.9 ± 1.1
70	Cape Bouvard (WA)	5	07:35	06:36	19:20	82	284	17.2 ± 0.5
71	Bunbury (WA)	5	08:10	07:11	21:10	184	1,379	18.0 ± 0.9
72	Busselton (WA)	5	08:00	07:01	21:20	120	442	23.3 ± 1.2
73	Albany (WA)	5	08:30	07:31	08:20 <sup>b</sup>	37	66	21.0 ± 1.9
74	Esperance (WA)	1	08:59 (18:05)	08:00 (17:06)	23:28	85	306	21.4 ± 1.9
75	Thevenard (SA)	1	11:35 <sup>a</sup> (20:25)	10:36 <sup>a</sup> (19:26)	00:07 <sup>b</sup>	18	13	30.5 ± 5.1
76	Port Stanvac (SA)	1	11:46 <sup>a</sup> (20:18)	10:47 <sup>a</sup> (19:19)	20:01	11	4	17.3 ± 0.7
77	Victor Harbor (SA)	5	11:20 <sup>a</sup> (19:25)	10:21 <sup>a</sup> (18:26)	03:25 <sup>b</sup>	63	175	16.1 ± 0.7
78	Portland (VIC)	1	10:48 <sup>a</sup> (18:54)	09:49 <sup>a</sup> (17:55)	01:19 <sup>b</sup>	93	438	18.1 ± 1.5

$\Delta t$  is the sampling interval for the gauge. The Australian states and territories are given in brackets: WA (Western Australia), SA (Southern Australia), and VIC (Victoria). The arrival and travel times provided in brackets for stations 72–76 located on the southern coast of Australia are for the second train of tsunami waves which were much higher and more readily resolved than the first train of waves

<sup>a</sup> Uncertain arrival

<sup>b</sup> 27th December

The 2004 waves were also recorded by two DART<sup>8</sup> and two ODP CORK<sup>9</sup> open-ocean bottom pressure stations located in the northeastern Pacific offshore from the coasts of Oregon, Washington and southern Vancouver Island (Fig. 1g) (RABINOVICH *et al.*, 2011). Moving further northwestward, the tsunami waves reached Alaska and then turned to the west, subsequently arriving at the Aleutian and northern Kuril islands (RABINOVICH *et al.*, 2006).

<sup>8</sup> DART = Deep-ocean assessment and reporting of tsunamis is the real-time open-ocean monitoring system developed by the Pacific Marine Environmental Laboratory, Seattle, WA (USA) for effective tsunami forecasting (<http://nctr.pmel.noaa.gov/Dart/>).

<sup>9</sup> ODP CORK = Ocean Drilling Program, Circulation Obviation Retrofit Kit is a long term seafloor observatory designed to record various geophysical and hydrophysical parameters in seabed boreholes.

According to our analyses, the tsunami wave field propagating through the southeastern Indian Ocean into the Pacific Ocean was much more complicated than that propagating into the remaining sectors of the Indian Ocean and into the Atlantic Ocean. Tsunami waves propagated from the source area to remote regions of the Pacific by various routes. These different routes, such as those associated with minimum travel distance, minimum travel time, or maximum energy conservation, resulted in differences in the integrated effects on the propagating waves. Additional complexity to the wave fields and subsequent observed tsunami records arose from multiple reflections from mainland coasts and large-scale bottom topographic features.

As noted in Sect. 2, the tide gauge networks in the Pacific Ocean and around the coast of Australia are

Table 6

*Tsunami characteristics for 24 Australian tide gauge stations located in the Pacific Ocean (isolated island stations are written in italics)*

No.	Station	$\Delta t$ (min)	First wave		Maximum wave		Energy	
			Arrival time (UTC)	Travel time (h:min)	Observ. time (UTC)	Height (cm)	$E_0$ (cm <sup>2</sup> )	Decay time, $t_0$ (h)
79	<i>Macquire Island (TAS)</i>	3	12:27 <sup>a</sup>	11:28 <sup>a</sup>	22:09	18	12	21.0 ± 2.7
80	Burnie (TAS)	1	20:46	19:47	10:24 <sup>b</sup>	34	34	22.7 ± 2.8
81	Spring Bay (TAS)	1	19:31	18:32	21:52	66	204	25.3 ± 2.8
82	Eden (NSW)	15	20:15	19:16	01:30 <sup>b</sup>	50	153	23.1 ± 1.2
83	Port Kembla (NSW)	1	18:37	17:38	05:58 <sup>b</sup>	57	124	16.3 ± 0.9
84	Sydney (NSW)	15	18:45	17:46	08:30 <sup>b</sup>	20	26	17.2 ± 1.7
85	<i>Lord Howe Island (NSW)</i>	15	23:30 <sup>a</sup>	22:31 <sup>a</sup>	09:45 <sup>b</sup>	38	52	19.7 ± 3.0
86	Port Office (QLD)	10	19:00 <sup>a</sup>	18:01 <sup>a</sup>	10:00 <sup>b</sup>	24	9	27.8 ± 5.8
87	Gateway Bridge (QLD)	10	18:20 <sup>a</sup>	17:21 <sup>a</sup>	09:20 <sup>b</sup>	21	7	28.5 ± 4.5
88	Brisbane (QLD)	10	18:10 <sup>a</sup>	17:11 <sup>a</sup>	09:30 <sup>b</sup>	21	7	27.1 ± 5.1
89	Mooloolaba (QLD)	10	22:00 <sup>a</sup>	21:01 <sup>a</sup>	13:30 <sup>b</sup>	19	14	35.4 ± 3.6
90	Bundaberg (QLD)	10	01:20 <sup>ab</sup>	24:21 <sup>a</sup>	17:50 <sup>b</sup>	19	10	27.8 ± 5.5
91	Burnett Heads (QLD)	10	01:10 <sup>ab</sup>	24:11 <sup>a</sup>	17:40 <sup>b</sup>	19	11	28.9 ± 3.9
92	Port Alma (QLD)	10	03:40 <sup>ab</sup>	26:41 <sup>a</sup>	11:40 <sup>b</sup>	10	–	26.2 ± 5.3
93	Rosslyn Bay (QLD)	1	03:53 <sup>ab</sup>	26:54 <sup>a</sup>	11:37 <sup>b</sup>	27	24	15.6 ± 2.9
94	Mackay (QLD)	10	05:30 <sup>ab</sup>	28:31 <sup>a</sup>	12:50 <sup>b</sup>	9	4	35.1 ± 5.7
95	Shute Harbour (QLD)	10	06:30 <sup>ab</sup>	29:31 <sup>a</sup>	11:30 <sup>b</sup>	10	3	36.1 ± 3.6
96	Bowen (QLD)	10	05:50 <sup>ab</sup>	28:51 <sup>a</sup>	20:10 <sup>b</sup>	13	6	32.8 ± 10.0
97	Cape Fergusson (QLD)	1	05:28 <sup>ab</sup>	28:29 <sup>a</sup>	00:14 <sup>c</sup>	8	3	31.6 ± 2.6
98	Cardwell (QLD)	10	06:10 <sup>ab</sup>	29:11 <sup>a</sup>	19:30 <sup>c</sup>	10	3	31.5 ± 14.7
99	Clump Point (QLD)	10	06:10 <sup>ab</sup>	29:11 <sup>a</sup>	04:00 <sup>c</sup>	12	4	29.4 ± 3.5
100	Mourilyan (QLD)	10	05:40 <sup>ab</sup>	28:41 <sup>a</sup>	12:10 <sup>b</sup>	9	4	29.3 ± 5.0
101	Cairns (QLD)	10	05:40 <sup>ab</sup>	28:41 <sup>a</sup>	16:41 <sup>b</sup>	9	3	–
102	Port Douglas (QLD)	10	06:00 <sup>ab</sup>	29:01 <sup>a</sup>	13:30 <sup>c</sup>	13	3	–

$\Delta t$  is the sampling rate for the gauge. Australian states and territories are given in the brackets: TAS (Tasmania), NSW (New South Wales), and QLD (Queensland)

<sup>a</sup> Uncertain arrival

<sup>b</sup> 27th December

<sup>c</sup> 28th December

much more extensive than in the Atlantic Ocean and in the non-Australian part of the Indian Ocean. Moreover, most tide gauges in the Pacific are designed to measure tsunami waves, which are much more common in this ocean than in any other ocean (c.f. GUSIAKOV, 2009). This is one of the reasons why, despite the fact that the “eastern” tsunami flux was less energetic than the “western” flux, the 2004 Sumatra tsunami was recorded by many more “eastern” tide gauges (from which we have identified 118 records as suitable for the present analysis).

Figure 1 indicates that there are several areas, such as Australia (Fig. 1e), New Zealand (Fig. 1f), and South and North America (Fig. 1h, g), with relatively large numbers of tide gauges. Using these areas, we divided the eastern stations into groups of

stations and present the estimated tsunami parameters for each group in individual tables.

#### 4.2.1 Australia

We used a total of 47 Australian stations (Figs. 1e, I and II) to examine the tsunami wave field in this region. The principal tsunami parameters for stations located on the coasts of Western Australia, Southern Australia, and Victoria are shown in Table 5, while those for Tasmania, New South Wales, and Queensland are presented in Table 6. The former group of stations is specific to the Indian Ocean while stations in the latter group (except Burnie) are specific to the Pacific Ocean. The Tasmanian station Burnie (41° 03' S; 145° 57' E) is formally located in the Indian Ocean

(delineated from the Pacific by the  $146^{\circ} 55'$  E meridian) but has been included with the parameters into Table 6 to keep all Tasmanian stations together.

There are significant differences in the characteristics of tsunami waves recorded on the different coasts of Australia. On the western coast from Port Hedland to Busselton (Table 5; Fig. 1-I)—the coast most exposed to arriving tsunami waves—the recorded waves were strongly prevalent and of high amplitude (except at Perth); at most stations, the maximum wave heights were higher than 80–100 cm and at two stations, Bunbury and Geraldton, as high as 184 and 157 cm, respectively. The calculated energy indices,  $E_0$ , are mainly in the 100–600 cm<sup>2</sup> range, while at Bunbury and Geraldton they are more than 1,000 cm<sup>2</sup> (1,379 and 1,123 cm<sup>2</sup>, respectively). As shown by Fig. 5 from Trrov *et al.* (2005), the observed  $E_0$  are generally in good agreement with the results of numerical simulations. The tsunami travel times (mainly from 5.5–7.5 h) matched well the computed travel times (Figs. 1, 5); at almost all stations, the first wave was positive indicating that this wave came from the “external” (oceanic) side of the initial dipole tsunami source disturbance.

On the southern coast (from Albany to Portland; Figs. 1e, “I”), the tsunami signal was quite different from that on the western coast. There were two trains of waves on the southern coast with the second wave train at all stations (except the westernmost station, Albany) the most predominant. Moreover, the first train rapidly weakened in the eastward direction, eventually becoming undetectable. The travel time of the first train was close to the theoretical value (Fig. 1e), while the second train arrived at the sites some 8–9 h later. It was the second wave train that had the maximum wave heights (from 11 to 93 cm).

The arrival times of the observed waves on the east coast of Australia (Table 6) were 4–14 h later than the theoretical time (Figs. 1e and 1-II), indicating that the first train either had not reached this coast or had arrived but was undetectable. Maximum wave heights of 34–66 cm were recorded on the coasts of Tasmania and New South Wales and the associated  $E_0$  values were 34–204 cm<sup>2</sup>; much smaller wave heights (8–27 cm) and energy indices (3–24 cm<sup>2</sup>) were observed on the coast of Queensland (Figs. 1-II and 5b).

The recorded tsunami characteristics on the western coast differed from those on the southern and eastern coasts because of the former’s exposure to the arriving tsunami waves (the latter two were lee coasts), and also because of specific topographic features of the Australian region. The broad and shallow Naturaliste Plateau located near the southwestern corner of Australia appeared to effectively slow down and reflect tsunami waves arriving from the source, allowing only a small portion of the arriving tsunami energy to pass through to the southern coast and to be recorded there as the “first train”. The main energy flux circumnavigated the plateau and then travelled along the Southeast Indian Ridge (indicated by a symbol “1” in Fig. 5); the second (highly energetic) wave train observed at southern stations was probably associated with waves that followed this route. Similarly, Tasmania Island and the extensive South Tasmania Rise sheltered the eastern Australian coast. Additional protection of the northeastern (Queensland) coast was provided by the Great Barrier Reef, an observational result supported by the numerical model computations (see Fig. 5b).

No tsunami waves were identified on the northern coast of Australia. Even at station Broomie located on the northwestern coast, relatively close to the source area (Fig. 1e), the tsunami signal was quite weak (Table 5). Apparently, the wide shallow-water shelf adjacent to the northern and northwestern coasts of Australia effectively reflected the arriving tsunami waves.

Tsunami waves recorded at island stations Cocos and Macquire (c.f. Fig. 1a) were readily detectable but not very high (59 cm at Cocos, Table 5; and 18 cm at Macquire Island, Table 6). According to our analysis, the arrival times at these stations were in good agreement with the theoretical travel times (Fig. 1a), demonstrating that the islands lay in the path of the main branch of tsunami wave flux. In contrast, the first tsunami waves at Lord Howe Island, located 600 km off the eastern mainland Australian coast (Fig. 1e), were detected approximately 10 h later than expected, apparently because they took a convoluted route to the recording site.



Table 7

*Tsunami characteristics for 29 New Zealand (NZ) tide gauge stations including those located on the Antarctic coast (isolated island stations are written in italics)*

No.	Station	$\Delta t$ (min)	First wave		Maximum wave		Energy	
			Arrival time (UTC)	Travel time (h:min)	Observ. time (UTC)	Height (cm)	$E_0$ (cm <sup>2</sup> )	Decay time, $t_0$ (h)
103	Jackson Bay ( <i>SI, W</i> )	1	15:10 (20:32)	14:11 (19:33)	09:57 <sup>a</sup>	91	253	26.6 ± 2.5
104	Dog Island ( <i>SI, S</i> )	1	15:35 (23:29)	14:36 (22:30)	06:15 <sup>a</sup>	58	95	21.3 ± 1.9
105	Bluff ( <i>SI, S</i> )	5	16:00 (23:50)	15:01 (22:51)	03:55 <sup>a</sup>	30	35	23.3 ± 2.4
106	Green Is ( <i>SI, E</i> )	5	18:00 <sup>b</sup> (00:20 <sup>a</sup> )	17:01 <sup>b</sup> (23:21)	16:25 <sup>a</sup>	49	95	24.5 ± 1.8
107	Otago ( <i>SI, E</i> )	1	17:44 (22:03)	16:45 (21:04)	10:24 <sup>a</sup>	33	39	38.3 ± 3.7
108	Timaru ( <i>SI, E</i> )	1	17:52 <sup>b</sup> (02:28 <sup>a</sup> )	16:53 <sup>b</sup> (25:29)	13:52 <sup>a</sup>	108	286	23.3 ± 1.4
109	Lyttelton ( <i>SI, E</i> )	1	20:22 <sup>b</sup> (03:03 <sup>a</sup> )	19:23 <sup>b</sup> (26:04)	06:30 <sup>a</sup>	63	94	20.5 ± 4.2
110	Sumner Head ( <i>SI, E</i> )	1	20:05 <sup>b</sup> (02:43 <sup>a</sup> )	19:06 <sup>b</sup> (25:44)	07:59 <sup>a</sup>	55	127	37.6 ± 5.3
111	Kaikoura ( <i>SI, E</i> )	1	19:16 <sup>b</sup> (04:19 <sup>a</sup> )	18:17 <sup>b</sup> (27:20)	16:12 <sup>a</sup>	53	120	14.3 ± 8.2
112	Charleston ( <i>SI, W</i> )	5	18:55 <sup>b</sup> (22:40)	17:56 <sup>b</sup> (21:41)	08:25 <sup>a</sup>	67	184	15.6 ± 1.3
113	Nelson ( <i>SI, N</i> )	1	20:38 <sup>b</sup> (02:39 <sup>a</sup> )	19:39 <sup>b</sup> (25:40)	16:50 <sup>a</sup>	67	127	21.9 ± 4.9
114	Little Kaiteriter ( <i>SI, N</i> )	1	20:30 (02:01 <sup>a</sup> )	19:31 (25:02)	15:51 <sup>a</sup>	61	146	18.5 ± 6.7
115	Wellington ( <i>NI, S</i> )	1	20:26 <sup>b</sup> (01:17 <sup>a</sup> )	19:27 <sup>b</sup> (24:18)	17:33 <sup>b</sup>	28	65	22.1 ± 6.0
116	Kapiti Island ( <i>NI, S</i> )	5	19:20 <sup>b</sup> (03:35 <sup>a</sup> )	18:21 <sup>b</sup> (26:36)	21:30 <sup>a</sup>	46	78	16.7 ± 2.0
117	Napier ( <i>NI, E</i> )	1	20:27 <sup>b</sup> (02:50 <sup>a</sup> )	19:28 <sup>b</sup> (25:51)	13:09 <sup>a</sup>	73	171	42.4 ± 11.9
118	Gisborne ( <i>NI, E</i> )	1	19:01	18:02	00:44 <sup>c</sup>	40	65	43.4 ± 10.5
119	Taranaki ( <i>NI, W</i> )	1	21:52 <sup>b</sup>	20:53	12:16 <sup>a</sup>	71	163	18.0 ± 1.0
120	Poutu Point ( <i>NI, W</i> )	5	21:50	20:56	08:40 <sup>a</sup>	27	25	16.6 ± 3.7
121	Anawhata ( <i>NI, W</i> )	5	22:15	21:16	02:10 <sup>a</sup>	54	91	15.6 ± 0.6
122	Manukau ( <i>NI, W</i> )	1	22:33	21:34	18:47 <sup>a</sup>	38	28	17.4 ± 1.7
123	Kaipara ( <i>NI, W</i> )	5	23:30	22:31	11:00 <sup>a</sup>	27	79	–
124	Whitianga ( <i>NI, N</i> )	5	01:05 <sup>a</sup>	24:06	20:30 <sup>a</sup>	36	75	30.7 ± 7.8
125	Moturiki Is-Maunganui ( <i>NI, N</i> )	5	03:45 <sup>a</sup>	26:46	09:00 <sup>a</sup>	14	7	48.0 ± 8.3
126	Waitemata ( <i>NI, N</i> )	1	03:46 <sup>a</sup>	26:47	07:49 <sup>a</sup>	12	10	–
127	Whangarei ( <i>NI, N</i> )	1	00:45 <sup>a</sup>	23:46	13:02 <sup>a</sup>	28	32	–
128	Marsden Point ( <i>NI, N</i> )	5	00:40 <sup>a</sup>	23:41	17:00 <sup>a</sup>	15	11	32.3 ± 2.4
129	<i>Kaingaroa (Chatham Is.)</i>	1	15:38 (23:11)	14:39 (22:12)	05:46 <sup>a</sup>	38	47	26.7 ± 2.5
130	Cape Roberts (Antarctica)	5	17:45	16:56	09:55 <sup>a</sup>	19	11	14.4 ± 3.0
131	Scott Base (Antarctica)	5	18:55	17:59	03:25 <sup>a</sup>	9	3	19.9 ± 2.0

*SI* South Island, *NI* North Island; “S”, “E”, “N” and “W” indicate southern, eastern, northern and western coasts of the islands, respectively.  $\Delta t$  is the sampling rate for the gauge

<sup>a</sup> 27th December

<sup>b</sup> Uncertain arrival

<sup>c</sup> 29th December

#### 4.2.2 New Zealand

This group includes 26 New Zealand (NZ) stations located on the mainland coast (Fig. 1f), a NZ island station, Kaingaroa, and two Antarctic NZ stations, Cape Roberts and Scott Base, located in the vicinity of the Ross Ice Shelf, about 10,000 km from the tsunami source (Fig. 1a). Estimated tsunami parameters for all 29 NZ stations are presented in Table 7. Most of these stations are located on the open coast and are highly exposed to pronounced wind waves and swell (and associated energetic IG-waves)

common to exposed Pacific regions, especially the west coast. Because of wind-generated IG-waves, tide gauge records in this region are typically very noisy and estimation of tsunami parameters, particularly the exact tsunami arrival times, is difficult. To suppress IG-waves, we used low-pass Kaiser-Bessel windows with window lengths ranging from 6 to 20 min, depending on the noise level. To better determine the arrival times, we worked with a group of stations simultaneously and within the group identified features that were likely associated with the first train of incoming tsunami waves.

Table 8

*Tsunami characteristics for 14 South American tide gauge stations (isolated island stations are written in italics)*

No.	Station	$\Delta t$ (min)	First wave		Maximum wave		Energy	
			Arrival time (UTC)	Travel time (h:min)	Observ. time (UTC)	Height (cm)	$E_0$ (cm <sup>2</sup> )	Decay time, $t_0$ (h)
132	<i>Easter (Pascua) Island (Chile)</i>	2	01:00 <sup>a</sup>	24:01	12:02 <sup>a</sup>	39	28	26.1 ± 2.4
133	<i>Juan Fernandez Island (Chile)</i>	2	00:47 <sup>a</sup>	23:48	16:04 <sup>a</sup>	8	2	33.0 ± 2.6
134	<i>San Felix Island (Chile)</i>	2	01:57 <sup>a</sup>	24:58	07:34 <sup>a</sup>	10	4	23.5 ± 2.7
135	Corral (Chile)	2	00:54 <sup>a</sup>	23:55	15:20 <sup>a</sup>	29	33	32.8 ± 3.7
136	Talcahuano (Chile)	2	01:38 <sup>a</sup>	24:39	01:08 <sup>b</sup>	42	66	30.5 ± 3.6
137	San Antonio (Chile)	2	00:30 <sup>a</sup>	23:31	03:38 <sup>b</sup>	15	9	24.1 ± 3.9
138	Valparaiso (Chile)	2	01:00 <sup>a</sup>	24:01	14:54 <sup>a</sup>	18	17	31.7 ± 5.5
139	Coquimbo (Chile)	2	02:02 <sup>a</sup>	25:03	16:02 <sup>a</sup>	35	51	29.0 ± 4.7
140	Caldera (Chile)	2	02:12 <sup>a</sup>	25:13	20:56 <sup>a</sup>	22	24	27.5 ± 7.2
141	Antofagasta (Chile)	2	03:32 <sup>a</sup> (10:26 <sup>b</sup> )	26:33 (33:27)	12:40	26	32	28.8 ± 3.3
142	Iquique (Chile)	2	03:44 <sup>a</sup>	26:45	05:12 <sup>b</sup>	24	18	37.4 ± 11.7
143	Arica (Chile)	2	04:13 <sup>a</sup> (13:20 <sup>b</sup> )	27:14 (36:21)	19:04 <sup>a</sup>	72	161	26.4 ± 8.9
144	Callao (Peru)	2	05:46 <sup>a</sup>	28:47	16:08 <sup>a</sup>	67	115	24.6 ± 3.1
145	<i>Baltra, Galapagos Is. (Ecuador)</i>	2	06:06 <sup>a</sup>	29:07	14:16 <sup>a</sup>	35	41	22.5 ± 1.5

$\Delta t$  is the sampling rate for the gauge

<sup>a</sup> 27th December

<sup>b</sup> 28th December

Significant tsunami waves were recorded on the NZ coast. At most stations on the South Island and the southern part of the North Island, maximum wave heights were >50 cm. At Timaru and Jackson Bay, waves reached 108 and 91 cm, respectively. Energy indices,  $E_0$ , ranged from 28 cm<sup>2</sup> at Wellington to 286 cm<sup>2</sup> at Timaru (Table 7). In many respects, the tsunami records at the NZ stations and island station Kaingaroa were similar to those for the southern coast of Australia in that there were two trains of waves, with the second train much more pronounced and energetic than the first. Maximum waves were related to the second train. The first train arrival was in reasonable agreement with the theoretical arrival time (Table 7; Fig. 1f), whereas the second train arrived 5–8 h later. The causes for the tsunami propagation behaviour are apparently the same as for the Australian coast whereby the first wave train was associated with the quickest travel route, while the second train was associated with a more convoluted, and more energy conserving, route.

At the northern stations (those from Gisborne to Marsden Point), the observed tsunami waves were less energetic, with maximum wave heights ranging from 12 to 54 cm and energy indices from 7 to

79 cm<sup>2</sup> (Table 7). This region was a “shadow” zone for incoming tsunami waves (Fig. 5c). Detectable tsunami waves arrived at the northern coastal stations 7–10 h later than had been predicted (Fig. 1f), similar to the delay in the “second train” at the southern stations.

Surprisingly well defined, but not very high, tsunami waves of 19 and 9 cm were recorded at the remote NZ Antarctic stations of Cape Roberts and Scott Base, respectively. The observed travel time (17–18 h) was in close agreement with the predicted travel time (16.5–17 h; Fig. 1a); the first wave consisted of a small trough followed by a much larger crest wave.

#### 4.2.3 South America

The group of South American stations includes 10 mainland stations (nine Chilean stations and Callao, Peru) and four island stations: San Felix, Juan Fernandez, Easter (all Chilean) and Baltra, the Galapagos Islands (Ecuador). Positions of the latter two stations are shown in Fig. 1a, while all the others are shown in Fig. 1h. Estimated tsunami parameters for all stations are presented in Table 8.

In general, tsunami oscillations were evident at all stations and the estimated parameters mutually consistent. The maximum wave heights (72 and 67 cm) and the largest energy indices (161 and 115 cm<sup>2</sup>) were observed at Arica (Chile) and Callao (Peru), respectively. The observed arrival times for stations within this group increased gradually in the northward direction and were 1–2 h later than predicted. The general character of the observed arrival times indicate that waves in the southern part of the Pacific Ocean did not cross the ocean in the northeastern direction, as had been originally expected (Fig. 1a), but instead travelled in a counterclockwise sense following the ocean ridges (indicated in Fig. 5a).

Pronounced second trains of tsunami oscillations were observed only at two stations: Antofagasta and Arica (Table 8). These trains, which had significantly stronger oscillations than the first trains, were recorded 7–9 h after the first wave arrival. At other stations, maximum wave heights were also observed much later (10–25 h) than the times for the first tsunami arrival but, unlike previously noted stations, did not arrive as distinct wave trains.

#### 4.2.4 North America

This group includes stations located on the western and northwestern coasts of North America (El Salvador, Mexico, California, British Columbia, Alaska and the Aleutian Islands) and the Russian station, Severo-Kurilsk, in the North Kuril Islands. Positions of the stations are shown in Fig. 1a and g; the primary estimated tsunami parameters are presented in Table 9. The 2004 tsunami records at these stations (as well as several other records in this region with weaker tsunami signals) were thoroughly analyzed by RABINOVICH *et al.* (2006) and focused on the general properties of the observed tsunami waves and their time–frequency evolution. Without going into details, we will highlight some of the important features of the recorded waves from the 2006 study.

As outlined by RABINOVICH *et al.* (2006), a specific feature of the tsunami records for North America was their marked train structure. Only the first and second train parameters have been included in Table 9; however, several more wave trains of waves were observed at most of the stations. These wave trains

contributed significant energy to the region and, as a result, pronounced tsunami “ringing” persisted at coastal stations for more than 4 days. Maximum recorded wave heights occurred mainly during the second wave train, with the height of 89.3 cm observed at Manzanillo (Mexico) representing the highest 2004 tsunami wave recorded in the Pacific Ocean. If we take into account the correction coefficient for 6-min sampling (Table 2), it is likely that the actual height of the Manzanillo wave was more than 1 m.<sup>10</sup>

A problem with the North American records is that many of them are very noisy due to the effects of local seiches and IG-waves (RABINOVICH *et al.*, 2006). Although we selected only stations with relatively large S/N ratios, accurate estimation of some tsunami parameters was problematic even for these stations. To suppress high-frequency oscillations and to simplify tsunami identification, we used the approach used for the NZ records, namely application of low-pass filters and analysis of a group of stations rather than individual stations. We also used wavelet analysis (see Figures 6, 9 and 12 RABINOVICH *et al.*, 2006) to enable us to examine variations of the observed tsunami waves in both frequency and time as well as to specify tsunami arrival times.

The complicated wave train structure of the recorded signals provided additional problems. Surprisingly, we found that while within one group of stations the wave trains had similar properties, the wave trains for another group could be markedly different. In other words, certain trains of waves arrived at some stations but not at others. Apparently, this peculiarity is related to the complicated character of the incoming waves which arrive by various routes and after multiple reflections from continental boundaries.

The 2004 Sumatra tsunami was distinctly recorded on the coast of California, with maximum wave heights of more than 50 cm at Crescent City (59 cm) and Port San Luis (52 cm), and more than

<sup>10</sup> After this paper had originally been submitted, Modesto Ortiz (CICESE, Ensenada, Mexico) kindly sent us the entire December 2004 record for this station. The 2-min sampling interval of these data enabled us to estimate more precisely the parameters of tsunami waves at this site (Table 9). The maximum recorded wave height was 101.1 cm, very close to what we had anticipated.

Table 9

*Tsunami characteristics for 16 North American and one Russian tide gauge stations (isolated island stations are written in italics)*

No.	Station	$\Delta t$ (min)	First wave		Maximum wave		Energy	
			Arrival time (UTC)	Travel time (h:min)	Observ. time (UTC)	Height (cm)	$E_0$ (cm <sup>2</sup> )	Decay time, $t_0$ (h)
146	Acajutla (El Salvador)	2	08:55 <sup>a</sup>	31:56	03:01 <sup>b</sup>	32	46	24.5 ± 0.2
147	Manzanillo (Mexico)	2	09:28 <sup>a</sup> (17:24 <sup>a</sup> )	32:29 (40:25)	19:56 <sup>a</sup>	101	587	30.3 ± 2.9
148	Cabo San Lucas (Mexico)	2	09:44 <sup>a</sup>	32:45	16:22 <sup>a</sup>	23	17	21.4 ± 11.2
149	Ensenada (Mexico)	1	06:18 <sup>ac</sup> (09:53 <sup>a</sup> )	29:19 <sup>c</sup> (32:54)	02:22 <sup>b</sup>	23	14	28.6 ± 2.4
150	San Diego (CA, USA)	1	05:14 <sup>ac</sup> (12:30 <sup>a</sup> )	28:15 <sup>c</sup> (35:31)	18:30 <sup>a</sup>	31	27	35.1 ± 8.4
151	La Jolla (CA, USA)	1	05:48 <sup>ac</sup> (12:12 <sup>a</sup> )	28:49 <sup>c</sup> (35:13 <sup>a</sup> )	19:24 <sup>a</sup>	15	4	30.6 ± 1.8
152	Port San Luis (CA, USA)	1	05:16 <sup>ac</sup> 12:22 <sup>a</sup>	26:17 <sup>c</sup> 35:23	20:53 <sup>a</sup>	52	87	27.6 ± 2.8
153	Point Reyes (CA, USA)	1	05:11 <sup>a</sup> (13:29 <sup>a</sup> )	28:12 (36:30)	22:25 <sup>a</sup>	36	58	28.1 ± 3.7
154	Arena Cove (CA, USA)	1	04:51 <sup>a</sup> (14:00 <sup>a</sup> )	27:52 (37:01)	17:42 <sup>a</sup>	31	34	30.7 ± 6.4
155	Crescent City (CA, USA)	1	05:20 <sup>a</sup> (13:38 <sup>a</sup> )	28:21 (36:39)	06:40 <sup>b</sup>	59	119	26.0 ± 3.4
156	Victoria (BC, Canada)	1	09:14 <sup>ac</sup> (15:29 <sup>a</sup> )	32:15 (38:30)	20:20 <sup>a</sup>	11	4	31.0 ± 4.0
157	Bamfield (BC, Canada)	1	08:56 <sup>a</sup>	31:57	20:19 <sup>a</sup>	6	3	39.0 ± 6.7
158	Tofino (BC, Canada)	1	08:48 <sup>a</sup> (16:00 <sup>a</sup> )	31:49 (39:01)	01:12 <sup>b</sup>	15	7	41.7 ± 4.5
159	Winter Harbour (BC, Canada)	1	08:45 <sup>a</sup> (12:16 <sup>a</sup> )	31:46 (35:17)	03:35 <sup>b</sup>	21	12	39.9 ± 2.7
160	<i>Adak (AK, USA)</i>	1	11:24 <sup>ac</sup> (15:14 <sup>a</sup> )	34:25 <sup>c</sup> (38:15)	18:06 <sup>a</sup>	20	19	32.3 ± 10.9
161	<i>Dutch Harbor (AK, USA)</i>	6	15:06 <sup>ac</sup>	38:07 <sup>c</sup>	20:12 <sup>a</sup>	13	9	34.7 ± 4.3
162	<i>Sand Point (AK, USA)</i>	6	12:30 <sup>a</sup> (15:48 <sup>a</sup> )	35:31 (38:49)	18:30 <sup>a</sup>	28	14	–
163	<i>Severo-Kurilsk (Russia)</i>	2	13:06 <sup>a</sup> (18:40 <sup>a</sup> )	36:07 (41:41)	07:00 <sup>b</sup>	31	34	32.7 ± 2.2

$\Delta t$  is the sampling rate for the gauge

<sup>a</sup> 27th December

<sup>b</sup> 28th December

<sup>c</sup> Uncertain

30 cm at Point Reyes (36 cm), San Diego (31 cm) and Arena Cove (31 cm). Perhaps even more impressive is the fact that the 2004 tsunami reached the northernmost part of the Pacific Ocean where it was observed at Sand Point, Dutch Harbor, Adak, and Severo-Kurilsk, more than 26,000 km from the source area (Table 9). With a mean wave speed  $c \sim 700\text{--}750 \text{ km h}^{-1}$ , it took the tsunami only about 1.5 days to propagate nearly 2/3 of the distance around the globe.

#### 4.2.5 Tropical Pacific Islands

In addition to continental regions, the 2004 Sumatra tsunami was recorded by tide gauges on a number of tropical Pacific islands from which we selected ten records with sufficient S/N ratio for further analysis (Fig. 1a; Table 10). Because most of these islands were located outside the main path of the tsunami energy flux (Fig. 5a), the observed tsunami waves were small, with wave heights ranging from 6 cm at Nuku Hiva (Marquesas Is.) to 34 cm at Kahului

(Oahu, Hawaiian Is.). Tsunami waves were clearly distinguishable at all 10 stations. We checked several other island stations (in addition to those shown in Table 10), in particular, Honiara (Solomon Is.), Betio (Kiribati), Majuro (Marshall Is.), Funafuti (Tuvalu), Apia (Western Samoa) and Rarotonga (NZ Cook Is.), but at all these islands the tsunami signal was poorly resolved or too weak to be examined. The fact that the tsunami travel times of  $\sim 21\text{--}27 \text{ h}$  were approximately 2–4 h longer than the theoretically estimated (see Fig. 1a) is likely attributable to the relatively convoluted trajectories the waves followed after leaving the source area.

#### 4.3. Energy Decay

The primary characteristics of the observed tsunami waves listed in Tables 3, 4, 5, 6, 7, 8, 9, 10 and the spatial distribution of the tsunami energy (Figs. 4, 5) reveal a rather complicated tsunami wave structure. Tide gauge data, supported by numerical simulation (TITOV *et al.*, 2005; KOWALIK *et al.*,

Table 10  
*Tsunami characteristics for 10 tropical Pacific Island stations*

No.	Station	$\Delta t$ (min)	First wave		Maximum wave		Energy	
			Arrival time (UTC)	Travel time (h:min)	Observ. time (UTC)	Height (cm)	$E_0$ (cm <sup>2</sup> )	Decay time, $t_0$ (h)
164	<i>Nukualofa (Tonga Is.)</i>	1	21:42	20:43	07:06 <sup>a</sup>	17	9	37.0 ± 2.3
165	<i>Nuku Hiva (Marquesas Is.)</i>	1	22:06	21:07	10:56 <sup>a</sup>	6	2	28.6 ± 3.1
166	<i>Port Vila (Vanuatu Is.)</i>	1	22:13 (00:03 <sup>a</sup> )	21:14 (23:04)	08:12 <sup>a</sup>	23	15	41.1 ± 2.7
167	<i>Suva (Fiji)</i>	1	22:48	21:49	03:59 <sup>a</sup>	12	7	19.7 ± 5.2
168	<i>Lautoka (Fiji)</i>	1	00:10 <sup>a</sup>	23:11	14:03 <sup>a</sup>	9	3	25.8 ± 4.7
169	<i>Pago Pago (US Samoa)</i>	1	23:20 <sup>b</sup> (03:59 <sup>a</sup> )	22:21 (27:00)	05:25 <sup>a</sup>	16	9	22.6 ± 5.9
170	<i>Kawaihae (Hawaii, USA)</i>	1	02:37 <sup>a</sup> (14:34 <sup>a</sup> )	25:38 (37:35)	19:36 <sup>a</sup>	14	6	27.3 ± 6.6
171	<i>Hilo (Hawaii, USA)</i>	1	03:36 <sup>a</sup> (15:05 <sup>a</sup> )	26:37 (38:06)	02:27 <sup>c</sup>	18	13	31.5 ± 1.9
172	<i>Honolulu (Hawaii, USA)</i>	1	03:41 <sup>a</sup> (14:39 <sup>a</sup> )	26:42 (37:40)	19:55 <sup>a</sup>	9	5	29.7 ± 4.2
173	<i>Kahului (Hawaii, USA)</i>	1	04:00 <sup>a</sup> (15:36 <sup>a</sup> )	27:01 (38:37)	02:26 <sup>c</sup>	34	42	26.8 ± 1.8

$\Delta t$  is the sampling rate for the gauge

<sup>a</sup> 27th December

<sup>b</sup> Uncertain

<sup>c</sup> 28th December

2007), demonstrate that the particular orientation of the earthquake seafloor rupture resulted in considerable anisotropic spreading of the 2004 Sumatra tsunami energy from the source area. In general, there is good agreement between simulated (TITOV *et al.*, 2005) and measured maximum waves, as indicated by the strong coincidence between computed “branches” of energy flux and zones of high recorded wave height (Figs. 4, 5). Although the 2004 tide gauge records reveal no simple relationship between observed wave height/energy index and distance from the source region, the wave property distributions possessed a definite spatial structure. Specifically, maximum wave heights in proximity to the source occurred near the beginning of the leading wave train, whereas for increasingly greater distances and wave propagation times, maximum waves occurred progressively later in the wave arrival sequence.

One of the more spectacular aspects of the far-field 2004 tsunami records for the North Atlantic and North Pacific oceans is their pronounced wave-train structure. Observations show that individual trains of incoming waves “pump” additional energy into the coastal regions, augmenting the local oscillations generated by the preceding tsunami wave trains. Global tsunami propagation models (TITOV *et al.*, 2005; KOWALIK *et al.*, 2007) reveal that these wave

trains are associated with wave refraction by large-scale seafloor topographic features and reflections from continental margins. Consequently, the energy decay of the 2004 tsunami waves was far from trivial. The marked lack of spatial uniformity in the tsunami decay was one of the first features that emerged from the 2004 tsunami records. RABINOVICH *et al.* (2006) wrote: “Tsunami energy decays quickly at stations closest to the source region (Hanimaadhoo, Male, and Colombo) and more gradually at stations located farther from the source... In general, the duration of tsunami ringing increases with increasing off-source distance, ranging from a few hours at Male (Maldives) to about two days at Salalah (Oman)”. In contrast, for remote records “A pronounced feature of the tsunami records at all sites (in the North Pacific) is the very long (>3.5 days) ringing”. Similarly, “...tsunami records in the North Atlantic had long (>4 days) ringing durations”.

The above qualitative conclusions were based on visual inspections of certain records and their frequency–time ( $f-t$ ) diagrams without specific estimation of the attenuation factors and decay times. The results of our comprehensive quantitative analysis of the 2004 tsunami energy decay confirm and expand on these preliminary conclusions. Estimated decay times for various regions are presented in the right column of Tables 3, 4, 5, 6, 7, 8, 9 and 10; their



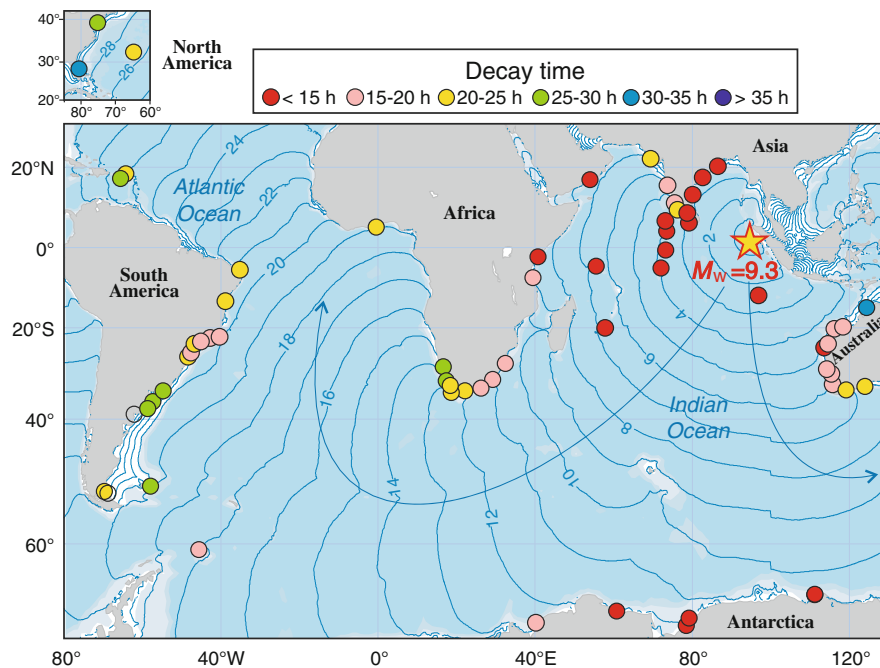


Figure 6

Map of the Indian and South Atlantic oceans showing the location of the  $M_w = 9.3$  Sumatra earthquake epicenter (star) and positions of tide gauges (coloured circles). Colours denote the tsunami decay time. Empty circles indicate stations where the decay time could not be estimated because the records are too short or the noise level too high. Solid thin blue lines are hourly isochrones of the tsunami travel time. The small inset above the main plot shows locations of three North Atlantic stations: Trident Pier, Atlantic City and the Bermuda Islands

spatial distribution is illustrated in Figs. 6 and 7. The absence of  $t_0$  values for some stations means that at these stations either the series were too short or too noisy.

The decay times ( $t_0$ ) estimated from the 27 stations in the Indian Ocean (Table 3) are mutually consistent: for 17 stations,  $t_0 = 12.8\text{--}15$  h; for 7 more,  $t_0 = 15\text{--}20$  h and for 3 stations  $t_0 = 20\text{--}22.5$  h. The maximum decay time  $t_0 = 22.5$  h occurred at Okha on the western coast of India. Apparently, it is not by accident, that sites with small  $t_0$  were located in the main corridor of the tsunami energy flux, while Okha and some other sites with larger  $t_0$  (c.f. Neendakara with  $t_0 = 20.9$  h) were in “tsunami shadow” zones (c.f. Figs. 4, 6).

The typical decay times  $t_0 = 20\text{--}27$  h for stations in the Atlantic Ocean (Table 4) are significantly longer than those in the Indian Ocean. Minimum  $t_0$  values are found for the northeastern coast of Brazil ( $t_0 = 18.0\text{--}20.2$  h at Arraial do Cabo, Ubatuba, Rio de Janeiro, Cananéia and Santos), while maximum  $t_0$  values are obtained for the North Atlantic

( $t_0 = 29.2\text{--}30.8$  h at Atlantic City, New Jersey; Trident Pier, Florida and Magueyes, Puerto Rico). All  $t_0$  values are considerably greater than the  $t_0 = 13.3$  h estimated by (VAN DORN, 1987) for the Atlantic Ocean.

As with the central region of the Indian Ocean (Table 3), the decay times on the west coast of Australia were mutually consistent. Typical  $t_0$  values were 16–20 h (Table 5), which is only slightly longer than for the east coast of India, the coast of Antarctica, and the tropical Indian Ocean islands (13–15 h) but similar to what was observed at the RSA coast. Roughly, the same values of  $t_0$  (16–20 h) were also observed along the eastern side of the southern Australian coast (Table 5) and on the southern part of the eastern coast (Table 6). However, for the southwestern (Busselton, Albany and Esperance) and southeastern (Tasmania) corners of Australia, the  $t_0$  values were markedly larger at 20–25 h (Tables 5, 6). Much longer decay times,  $t_0 = 27\text{--}36$  h, were observed on the northeastern (Queensland) coast of Australia (Table 6). In general,

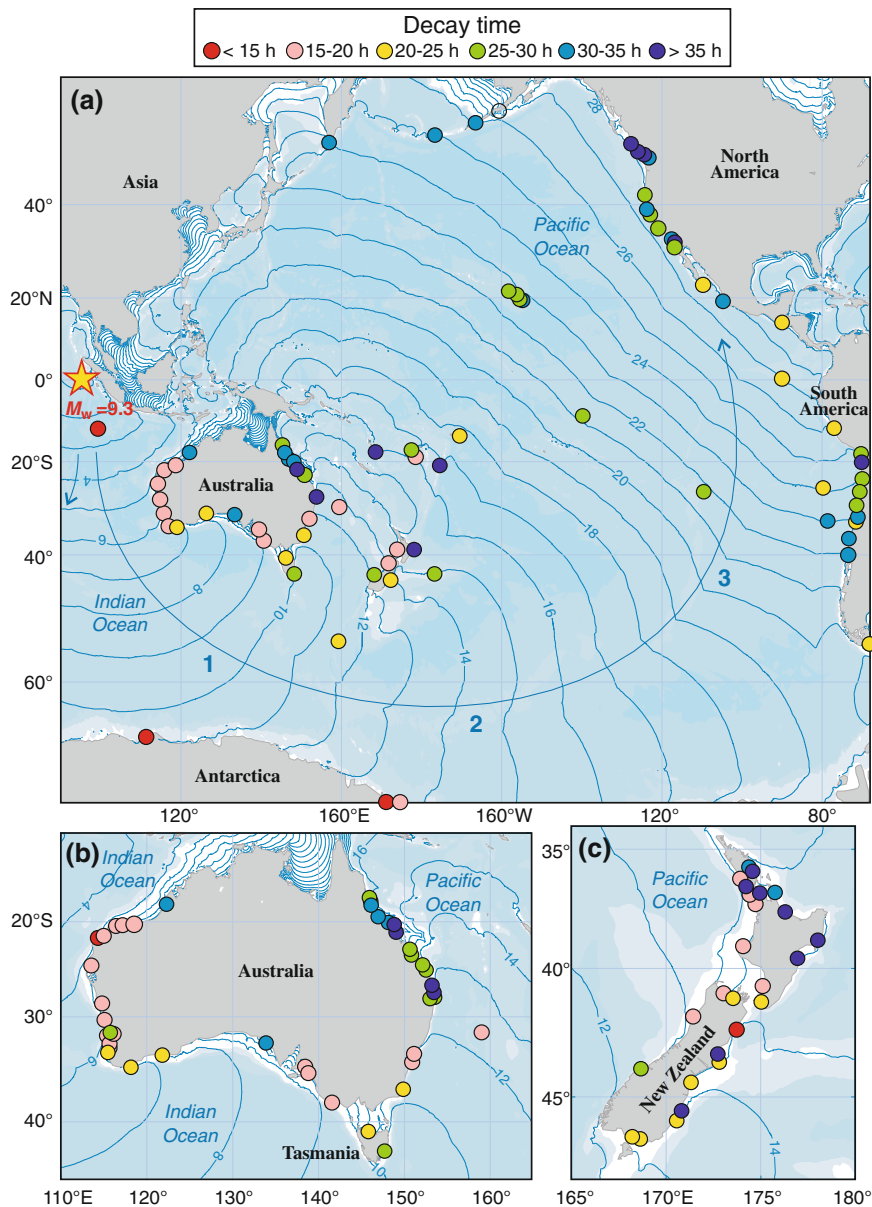


Figure 7

As for Fig. 6 but for the Pacific Ocean: **a** entire Pacific Ocean; **b** Australia; and **c** New Zealand. The curved blue arrow in **a** shows the direction of the “eastern” branch of the tsunami energy flux, while labels 1–3 indicate the Southeast Indian Ridge (“1”), Pacific Antarctic Ridge (“2”), and East Pacific Rise (“3”)

$t_0$  estimates for the coast of Australia confirm the significant influence of bottom topography and large-scale coastal geometry on the observed characteristics of tsunami waves, including the decay times (Fig. 6b).

The estimated tsunami energy decay for the coast of New Zealand (Table 7; Fig. 6c) is highly

complicated. One of the reasons for this is that the records from the stations located on the opposite coasts of two of the main islands are poorly correlated and have markedly different wave features. Local topographic effects may also contribute to energy conservation (or energy radiation) at specific sites. An additional important factor is the high noise level

related to storm-induced IG-waves which limit the accuracy of the tsunami property estimates, including  $t_0$ , at some stations located on the North Island. To simplify comparison of wave properties, for each station in Table 7 we indicated islands (South, SI; and North, NI) and coasts (southern, eastern, western and northern). At the South Island, the decay times were mainly between 21 and 27 h, except for Otago and Sumner Head, where the decay times increased to 38.3 and 37.6 h, respectively. At Kaikoura and Charleston, decays were down to 14.3 and 15.6 h, respectively. Along the coast of the North Island, decay times were relatively short on the western coast,  $t_0 = 15.6$ –18 h, and longer on the northern,  $t_0 = 30$ –48 h, and eastern,  $t_0 = 42$ –44 h, coasts (Fig. 6c). At an open ocean island station Kangaroo, located 800 km eastward from the main coast of New Zealand, the estimated decay time was about 27 h, while at the two NZ Antarctic stations, these times were 14–20 h (Table 7), close to what was observed at the Antarctic stations in the Indian Ocean (Table 3).

The South American stations (Table 8) had the same problems as the NZ stations: high noise level or/and too short tsunami records at some stations. For this reason, we were unable to estimate the decay times at Corral, Talcahuano and Coquimbo, despite the fact that tsunami oscillations were quite significant at these stations. In general, the decay times estimated for other stations (including island stations) were relatively consistent with  $t_0 = 22$ –29 h. Only at three stations, Juan Fernandez Island, Valparaiso and Iquique, was the estimated decay time longer than 30 h.

The main problem for selected North American records is the high background noise level. Despite this problem, the tsunami signal was clear enough to enable us to estimate decay times at all stations except Sand Point (Alaska) and to reveal a tendency for  $t_0$  to increase northward along the coast (Fig. 7a). At Central American, Mexican and California stations,  $t_0$  ranged from 21.4 h at Cabo San Lucas to 35.1 h at San Diego, with a mean  $t_0 = 28.3$  h for this group of stations. In contrast, for the Canadian stations located on the oceanic side of Vancouver Island, as well as for the two Aleutian and one Kuril Island stations,  $t_0$  was in the range of 31.0–41.7 h with a mean value of 35.9 h.

The last group of the stations are those in the tropical Pacific Ocean (Table 10). At most stations the tsunami signal was weak,  $<20$  cm (except at Kahului, Hawaii and Port Vila, Vanuatu). For the Hawaiian group of stations, decay times were fairly consistent, ranging from 26.8 h for Kahului to 31.5 h for Hilo. This contrasts with other Pacific Island stations for which decay times were much more variable, ranging from 19.7 h at Suva (Fiji Is) to 41.1 h at Port Vila (Vanuatu Is), probably due to very complicated bottom topography in the region of Tonga–Vanuatu–Fiji–Samoa islands and associated strong tsunami wave reflection, refraction and trapping.

## 5. Discussion and Conclusions

Our analysis reveals considerable spatial heterogeneity in the tsunami decay time,  $t_0$ . This contradicts MUNK (1963) and VAN DORN (1984, 1987) who hypothesized that tsunami decay time depends only on the morphometric characteristics of oceanic basins, such as the mean water depth and lateral dimension, and should therefore be relatively uniform within a given basin (about 14 h for the Indian and Atlantic oceans and 22 h for the Pacific Ocean). According to Tables 3, 4, 5, 6, 7, 8, 9 and 10,  $t_0$  for the 2004 Sumatra tsunami was highly variable within the main ocean basins, ranging from 12.8 to 13.0 h at Mauritius and Maldives Islands to 22.5 h at Okha (India) in the Indian Ocean; from 18.0 h at Arraial do Cabo (Brazil) to 30–31 h at Trident Pier (Florida) and Magueyes (Puerto Rico) in the Atlantic Ocean, and from 15.6 h at Rosslyn Bay (Australia) to 42–48 h at stations on the North Island (New Zealand) and 39–42 h at stations on the west coast Vancouver Island (Canada) in the Pacific Ocean.

At first glance, the distribution of decay times in Tables 3, 4, 5, 6, 7, 8, 9 and 10 appears to be somewhat unstructured. However, closer examination of the global distributions reveals a definite spatial pattern. To provide a better visualization of this structure, we partitioned the calculated decay times into six distinct categories based on the observed rates of attenuation (coloured values in Figs. 6, 7). For the western group of stations, it is evident that,

for sites in the Indian Ocean exposed to tsunami waves arriving directly from the source region,  $t_0 < 15$  h. For the western coast (“shadow region”) of India and the southeastern coast of South Africa,  $t_0 = 15$ –20 h, while at remote stations in the Atlantic Ocean,  $t_0 = 20$ –30 h (Fig. 6). Thus, the observed decay times generally increase with distance and tsunami travel time,  $T_t$ . A similar structure is observed for the “eastern” group of stations. For example, at Cocos (the station nearest to the source),  $t_0 = 13$  h; decay times then increased to 15–20 h for the western (“exposed”) coast of Australia, to 15–25 h for the southern (“lee”) coast of Australia, and to  $t_0 > 25$  h for the northeastern coast of Australia (which is sheltered from the open Pacific by the Great Barrier Reef). Similarly,  $t_0 > 25$  h for the coasts of South and Central America, and increased to greater than 30–35 h for the most remote stations (those on the coasts of British Columbia and Alaska; Fig. 7).

The observed oceanic energy decay structure appears to have been related to ever-evolving properties of the wave trains during their cross and inter-ocean propagation. Global and regional topography clearly play major roles in the formation of far-field tsunami wave properties, and ultimately lead to convoluted wave structure and persistent ringing. Wave dispersion is an additional factor influencing far-field records and promoting long-duration ringing. In contrast, in near-field regions it is mainly the source configuration and orientation that determine the energy redistribution. Wave dispersion does not noticeably affect these records. The paucity of multiple tsunami pathways and reflections accounts for the relatively simple structure of tsunami records from near-field regions (see Fig. 4).

Figures 6 and 7 indicate that the travel time,  $T_t$ , is the key parameter determining the decay time of tsunami waves. The greater the distance from the source region, the longer the travel time and the more prolonged the “tsunami forcing” by the incoming tsunami wave energy. This distance-related forcing likely arises from three main factors: (1) an increase in the number of possible tsunami ray paths directed toward a given site (including those reflected from continental margins; c.f., SATAKE, 1988); (2) increased lag times between the “fastest” and

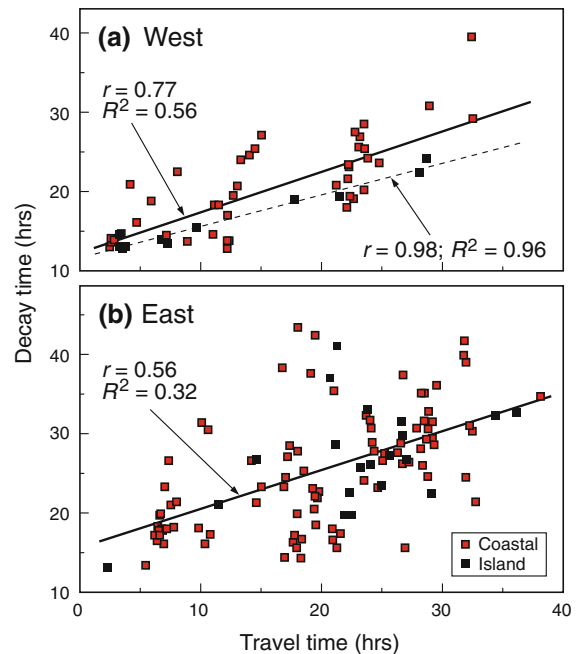


Figure 8

Scatter plots illustrating the correlation between the decay time,  $t_0$ , and the tsunami travel time,  $T_t$ , for **a** west and **b** east groups of stations. *Solid lines* denote regression lines for all west and east stations (continental and island stations together); the correlation coefficient,  $r$ , and the coefficient of determination,  $R^2$ , are indicated. Also shown are  $r$  and  $R^2$  for west group island stations

“slowest” rays from the source to the observational site; and (3) wave dispersion. The longer the tsunami forcing, the longer the “tsunami ringing”.

We applied a least squares method (c.f. EMERY and THOMSON, 2003) to model the relationship between the decay time  $t_0$  and the travel time  $T_t$ ; viz.

$$t_0 = aT_t + b, \quad (5)$$

where  $a$  and  $b$  are regression coefficients. Regression relationships were calculated for several specific groups of stations, namely the “west” and “east” groups and the “continental” and “island” groups (Fig. 8). For the “west” group of stations:

$$a = 0.51 \pm 0.12; \quad b = 12.3 \pm 2.1 \text{ h}; \quad r = 0.77; \\ R^2 = 0.59; \quad (6)$$

and for the “east” group:

$$a = 0.49 \pm 0.14; \quad b = 15.6 \pm 3.0 \text{ h}; \quad r = 0.56; \\ R^2 = 0.32, \quad (7)$$

where  $r$  is the correlation coefficient and  $R^2$  is the “correlation of determination”, which is a measure of the goodness of the regression model (EMERY and THOMSON, 2003). The regression model is statistically most significant for the “west” group (both  $r$  and  $R^2$  are considerably higher), apparently because the possible routes for tsunami waves propagating to the west into the Atlantic Ocean were much more direct (the waves were less affected by complicated coastal and bottom topography) than for the waves propagating to the east into the Pacific. As described in Sects. 3 and 4, there are several “east” regions (specifically, the southern and eastern coasts of Australia, New Zealand and Pacific tropical islands) that were characterized by late tsunami arrival times and by highly intricate and anomalous tsunami decay.

For the combined “west” and “east” continental stations:

$$a = 0.54 \pm 0.11; b = 14.1 \pm 2.3 \text{ h}; r = 0.63; \\ R^2 = 0.40; \quad (8)$$

and for the island stations:

$$a = 0.58 \pm 0.20; b = 12.2 \pm 4.3 \text{ h}; r = 0.74; \\ R^2 = 0.54 \quad (9)$$

Here,  $r$  and  $R^2$  are noticeably higher for the island stations, apparently because tsunamis arriving at the island stations were much less affected by local topographic effects. The contrast between island and continental stations is especially evident for the west group of stations for which  $r = 0.98$  and  $R^2 = 0.96$ , respectively; i.e., the relationship between travel time and decay time is almost functional. For the continental “west” stations, these values are significantly smaller (0.76 and 0.58, respectively) but still higher than for the “east” stations.

Although our results demonstrate a significant correlation between tsunami decay rate and travel time (i.e. the distance from the source), there is clearly considerable scatter in the regression estimates in (6–9), especially for continental stations, indicating that travel time is not the only factor affecting the decay of tsunami wave energy. The effect of large-scale topographic features on tsunami wave structure and attenuation is evident for some groups of stations. For example, it appears that the

anomalously protracted ringing and slow tsunami energy decay on the northeastern (Queensland) coast of Australia was linked to the Great Barrier Reef. The reef not only shelters the coast from tsunami waves arriving from the open ocean to the east but also contributes to the conservation of tsunami wave energy propagating along the shelf from the south. A different wave picture emerges for southern Australia. Here, the Great Australian Bight forms a vast protective “pocket” that causes the energy to decay in a markedly different and slower manner than for western Australia (Fig. 6b). In contrast, tsunami attenuation was significantly more rapid along the extensive “bight” adjoining the Pacific coast of Central America (Fig. 7) than along the adjacent coasts of South and North America.

Close examination of the tsunami data further reveals that the broader and shallower the continental shelf, the greater the incoming tsunami wave energy it can retain. This retention (or wave “capacitance”) leads, in turn, to more protracted tsunami ringing and to slower energy decay at adjacent coastal sites. This effect is quite pronounced for the Atlantic shelf of

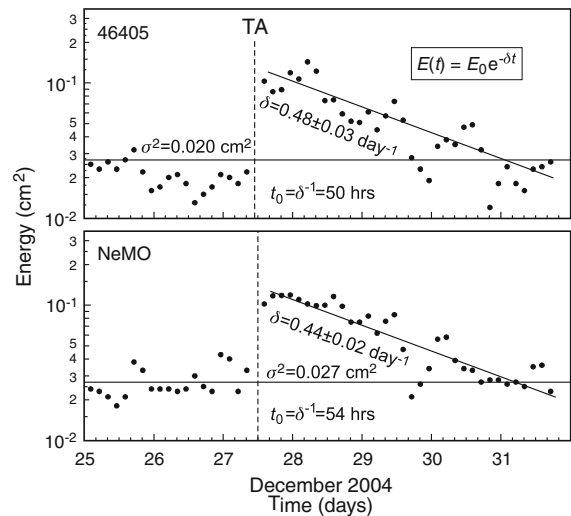


Figure 9

Temporal variations in the 2004 Sumatra tsunami energy in the northeast Pacific seaward of the Oregon coast. Bottom-pressure measurements with 15-s sampling were obtained by DART station 46405 (water depth 3,480 m) and NeMO (water depth 1,510 m) (see Fig. 1g for station positions). Dashed vertical lines labelled “TA” denote the tsunami arrival time; solid horizontal lines indicate the background noise level. Inclined solid lines are least squares fits to the variance decays



South America (Figs. 4, 6). For stations located on the Brazilian coast, such as Cananéia, Ubatuba, Arraial do Cabo, and Rio de Janeiro, the shelf is narrow and deep, and the decay time relatively short ( $t_0 = 18.0\text{--}19.6$  h). In contrast, for stations Mar del Plata and Santa Teresita (Argentina), La Paloma (Uruguay) and Port Stanley (Falkland Is) located on the broad, shallow Patagonian shelf, the decay times are relatively long ( $t_0 = 25.4\text{--}27.5$  h), which is roughly 1.4 times longer than for the Brazilian coast (Table 4). Tsunami waves arriving at the shelf from the open ocean, are partly reflected back to sea and partly absorbed by the shelf. The normalized propagation time,  $\hat{T}_s$ , responsible for this tsunami interaction with the shelf is

$$\hat{T}_s = \frac{T_s}{T} = \frac{1}{T} \left[ \int_L^0 \frac{dx}{\sqrt{gh(x)}} \right], \quad (10)$$

where  $T$  is the wave period  $T_s$  is the time required for tsunami waves propagate across the shelf in the  $x$  direction, and  $L$  and  $h(x)$  are the shelf width and depth, respectively. The greater  $\hat{T}_s$ , the greater the tsunami energy retained on the shelf and the lower the energy reflected back to the open ocean. For the southeastern Brazilian shelf,  $T_s \sim 1.0\text{--}1.5$  h, while for the Patagonian shelf  $T_s \sim 3.0\text{--}4.5$  h. Similarly, for typical wave periods  $T = 0.8$  h for these two regions,  $\hat{T}_s = 1.25\text{--}1.90$  and  $3.8\text{--}5.6$  h, respectively.

When he proposed his analogy between tsunami waves and sound waves in an enclosed room, MUNK (1963) did not consider the specific properties of the room's surfaces. The "ceiling", "floor", and "walls" were assumed to have the same acoustical response characteristics. Because of their convoluted shorelines, continental shelves, and seafloor, the basins of the World Ocean do not present such uniformity to seismically generated tsunamis. This is clearly evident in Figs. 6 and 7. In general, estimates of decay times for open-ocean island stations (with their relatively narrow shelves and, consequently, smaller  $\hat{T}_s$ ) more closely approximate the acoustical analogy of MUNK (1963) and VAN DORN (1984, 1987) than those for continental coastal stations. However, even within a given ocean basin, decay times for different island sites are far from uniform (Tables 3, 4, 5, 6, 7, 8, 9, 10). Moreover, regardless of their size and extent of

their adjacent shelf region, all islands also have bays, harbours and inlets where recorded tsunamis are affected by local resonant factors. For example, the wave spectra for Port Louis (Mauritius) for tsunamis and background oscillations both have prominent peaks at periods of 20 and 7.4 min and those for the Cocos Islands have major peaks at periods 21 and 14 min; all peaks are associated with local topographic resonance effects (RABINOVICH and THOMSON, 2007). Local resonant effects, together with wave trapping, affect wave attenuation at all mainland and island coastal tide gauge sites, with somewhat stronger effects at mainland sites.

Deep-ocean bottom pressure measurements, which are not affected by coastal resonant topographic effects (c.f. MOFJELD, 2009), provide the best opportunity to evaluate "pristine" tsunami energy decay times. Only these decay times can be compared directly to the estimates by MUNK (1963) and VAN DORN (1984, 1987) and to the time of tsunami wave propagation. The derivations of such decay times was made possible by bottom pressure data recorded by two DART (46405 and NeMO<sup>11</sup>) and two ODP CORK (1026 and 1301) stations in the northeastern Pacific (Fig. 1g) during the 2004 Sumatra tsunami (RABINOVICH *et al.*, 2011). Stations 46405 (water depth  $h = 3,480$  m) and NeMO ( $h = 1,510$  m) were separated by a distance of 337 km and had sampling intervals  $\Delta t = 15$  s. Stations 1026 ( $h = 2,658$  m;  $\Delta t = 15$  s) and 1301 ( $h = 2,658$  m;  $\Delta t = 1$  min) were located roughly 1 km apart and 271 km from NeMO. The waves from the 2004 event had heights of about 2 cm at these sites and arrived at the stations about 34–35 h after the main earthquake shock following a 21,000 km journey through the Indian and Pacific oceans. Another impressive property of the tsunami waves recorded at these sites was their long (>3.5 days) ringing.

The energy decay parameters for the deep northeast Pacific stations were calculated in the same way as for coastal tide gauges (Fig. 9). The estimated

<sup>11</sup> NeMO = New Millenium Observatory, a station with a precise BPR (the same as in DARTs), which was deployed near an active volcano located on the Juan de Fuca Ridge. The purpose of this station was to study the dynamic interactions between submarine volcanic activity and seafloor hotspots.



decay times for DART stations 46405 and NeMO were  $t_0 = 50.1 \pm 2.7$  and  $54.1 \pm 2.4$  h, respectively. The ODP CORK stations did not use sampling averaging and, consequently, possessed significantly higher instrumental noise and yielded considerably less accurate evaluated decay parameters. Nevertheless, the respective decay times of  $56.1 \pm 9.3$  h for site 1026 and  $60.9 \pm 12.2$  h for site 1301 were in reasonable agreement with the DART estimates. Assuming that the ODP CORK  $t_0$  values are over-estimates, the smaller DART estimates still give decay times that are 2.3–2.5 times longer than the  $e$ -folding decay time  $t_0 \approx 22$  h estimated by VAN DORN (1984, 1987) for the Pacific. One possible reason for this contradiction is that MUNK (1963) and VAN DORN (1984, 1987) used a *closed* room analogy, whereas the Indian, Atlantic and Pacific oceans have very wide “entrances” that connect them to one another. This suggests that the closed-room analogy is an over-simplification. Cross-spectral analysis of the 2004 DART and ODP CORK tsunami records indicates that the energy flux was from the south and had a long ( $\sim 3$  days) duration. Thus, it appears that the tsunami energy from the event radiated out from the Indian Ocean into the Atlantic and Pacific oceans, thus shortening tsunami attenuation time in the Indian Ocean but increasing it in the Atlantic and Pacific oceans. This is clearly the case in Figs. 6 and 7 which show relatively high  $t_0$  values for the Atlantic and Pacific oceans compared to the Indian Ocean.

The long duration 2004 tsunami decay times observed by deep-ocean instruments in the northeast Pacific do not appear to be associated with the absorption properties of the shelf discussed above but rather with distance from the source. Due to multiple reflections from the continental borders and various topographic irregularities, as well as refraction, scattering and dispersion, the propagating tsunami energy spreads not only in space but also in time. Far-field open-ocean tsunami measurements clearly demonstrate this effect.

As our analysis for the 2004 Sumatra tsunami illustrates, the energy decay of major trans-oceanic tsunamis is a much slower and more complicated process than previously reported. Large-scale topographic irregularities apparently play a principal role

in this process, with mid-ocean ridges serving as wave-guides that efficiently transmit tsunami energy from the source area to remote regions of the World Ocean (TITOV *et al.*, 2005; KOWALIK *et al.*, 2007). Moreover, broad continental shelves are especially capable of trapping a significant fraction of the incoming tsunami energy, leading to protracted tsunami ringing along the adjacent coast.

#### *Acknowledgments*

The data used in the present study were collected over more than 5 years. A great many institutions and individuals helped us search for the data. We gratefully acknowledge the following organizations for providing us with tide gauge records for the 2004 Sumatra tsunami: the University of Hawaii Sea Level Center (Honolulu, Hawaii, USA); the Pacific Tsunami Warning Center (Honolulu, Hawaii, USA); The West Coast and Alaska Tsunami Warning Center (Palmer, Alaska, USA); the National Tidal Centre and Australian Antarctic Division, Australian Bureau of Meteorology (Kent Town, South Australia); the Department of Transport—Government of Western Australia (Perth, WA); Maritime Safety Queensland, Department of Transport and Main Roads (Brisbane, Queensland, Australia); the National Institute of Water and Atmospheric Research (NIWA, Hamilton, New Zealand); the Center for Operational Oceanographic Products and Services (CO-OPS), National Ocean Service (NOS), the US National Atmospheric and Oceanic Administration, NOAA (Seattle, Washington, and Silver Spring, Maryland), the Canadian Hydrographic Service (Sidney, British Columbia and Halifax, Nova Scotia), the Permanent Service for Mean Sea Level (Liverpool, UK); the Hydrographic and Oceanographic Department, the Survey of India (Delhi), and the National Institute of Oceanography (Goa, India); the Japan Coast Guard (Tokyo); the Hydrographic Office of the Republic of South Africa (Tokai, RSA); the Servicio Hidrográfico y Oceanográfico de la Armada de Chile (SHOA, Valparaíso); the Departamento de Oceanografía, Universidade de São Paulo (Brazil); the Centro de Hidrografia da Marinha (Niteroi, Brazil); the Division Oceanografía Física (Montevideo, Uruguay); and the Departamento

Oceanografía, Servicio de Hidrografía (Buenos Aires, Argentina). We also thank those people who helped us obtain, assemble and verify these data; our specific thanks to Mark Merrifield (Honolulu, HI), Ruth Farre (Tokai, South Africa), Bill Mitchell (Adelaide, Australia), Mike Davis (Kent Town, Australia), Philip Woodworth (Liverpool, UK), Paul Whitmore (Palmer, AK, USA), Stuart Weinstein (Honolulu, HI, USA), Fred Stephenson, Denny Sinnott and Neil Sutherland (Sidney, BC, Canada), John Fleming, Jorge Cruz Cristóbal and Claudia Valenzuela Cuevas (Valparaíso, Chile), Tatiana Ivelskaya (Yuzhno-Skhalinsk, Russia), Kelly Stroker (Boulder, CO, USA), Marie Eble (Seattle, WA, USA), Natalia Donoho (Silver Spring, Md, USA), Modesto Ortiz (Ensenada, Mexico), K.A. Abdul Rasheed (Kochi, India), Carlos França (São Paulo, Brazil), Walter Dragani (Buenos Aires, Argentina), Ernesto Forbes (Montevideo, Uruguay), and Rosuita Roso (Niteroi, Brazil). We are most grateful for the incredible help we received from Paul Davill (Kent Town, Western Australia), Daryl Metters (Brisbane, Queensland), Derek Goring (Christchurch, NZ), and Rob Bell (Hamilton, NZ) in locating and incorporating numerous Australian and New Zealand data. We also thank Vasily Titov (PMEL/NOAA, Seattle, USA) for making available results of his numerical model, Isaac Fine (IOS, Sidney, Canada) for fruitful discussions, Maxim Krassovski (IOS, Sidney, Canada) for helping us with maps and Patricia Kimber (Sidney, Canada) for drawing the figures.

#### REFERENCES

- ABE, K. (2006), *Dominant periods of the 2004 Sumatra tsunami and the estimated source size*, Earth Planets Space 58, 217–221.
- BATTJES, J.A. (1988), *Surf-zone dynamics*, Annual Rev. Fluid Mech. 20, 257–293.
- CANDELLA, R.N., RABINOVICH, A.B., and THOMSON, R.E. (2008), *The 2004 Sumatra tsunami as recorded on the Atlantic coast of South America*, Advances in Geosciences 14 (1), 117–128.
- DRAGANI, W.C., D'ONOFRIO, E.E., GRISMEYER, W., and FIORE, M.E. (2006), *Tide gauge observations of the Indian ocean tsunami, December 26, 2004, in Buenos Aires coastal waters, Argentina*, Cont. Shelf Res. 26, 1543–1550.
- EMERY, W.J., and THOMSON, R.E. (2003), *Data Analysis Methods in Physical Oceanography*, 2<sup>nd</sup> and revised edition, Elsevier, New York.
- FINE, I.V., RABINOVICH, A.B., and THOMSON, R.E. (2005), *The dual source region for the 2004 Sumatra tsunami*, Geophys. Res. Lett. 32, L16602, doi:10.1029/2005GL023521.
- FRANÇA, C.A.S., and DE MESQUITA, A.R. (2007), *The December 26th 2004 tsunami recorded along the southeastern coast of Brazil*, Natural Hazards 40, 209–222.
- FUJII, Y. and SATAKE, K. (2007), *Tsunami source of the 2004 Sumatra-Andaman Earthquake inferred from tide gauge and satellite data*, Bull. Seism. Soc. Amer. 97 (1A), S192–S207.
- GORING, D. (2008), *Extracting long waves from tide gauge records*, J. Waterw. Port Coastal Ocean Engin., ASCE 134 (5), 306–312, doi:10.1061/(ASCE)0733-950X(2008) 134:5(306).
- GUSIAKOV, V.K. (2009), *Tsunami history: Recorded*, In: *The Sea*, Vol.15, *Tsunamis*, A. Robinson, E. Bernard (Eds.), Harvard University Press, Cambridge, USA, 23–53.
- HOLMAN, R.A., HUNTLEY, D.A., and BOWEN, A.J. (1978), *Infragravity waves in storm conditions*, Proc. 16<sup>th</sup> Coastal Eng. Conf., Hamburg, 268–284.
- KOVALEV, P.D., RABINOVICH, A.B., and SHEVCHENKO, G.V. (1991), *Investigation of long waves in the tsunami frequency band on the southwestern shelf of Kamchatka*, Natural Hazards 4, 141–159.
- KOWALIK, Z., KNIGHT W., LOGAN T., and WHITMORE P. (2007), *The tsunami of 26 December 2004: Numerical modeling and energy considerations*, Pure Appl. Geophys. 164, 379–393.
- LAY, T. et al. (2005), *The Great Sumatra-Andaman earthquake of 26 December 2004*, Science 308, 1127–1133.
- LEONARD, M. (2006), *Analysis of tide gauge records from the December 2004 Indian Ocean tsunami*, Geophys. Res. Lett. 33, L17602, doi:10.1029/2006GL026552.
- MELO, E., and ROCHA, C. (2005), *Sumatra tsunami detected in Southern Brazil*, Maritime Hydraulics Laboratory, Federal University of Santa Catarina, Brazil, Unpublished Report, <http://www.pmel.noaa.gov/tsunami/sumatra20041226.html>.
- MERRIFIELD, M.A., et al. (2005), *Tide gage observations of the Indian Ocean tsunami, December 26, 2004*, Geophys. Res. Lett. 32, L09603, doi:10.1029/2005GL022610.
- MILLER, G.R., MUNK, W.H., and SNODGRASS, F.E. (1962), *Long-period waves over California's continental borderland. Part II: Tsunamis*, J. Mar. Res. 20, 31–41.
- MOFJELD, H.O. (2009), *Tsunami measurements*, In: *The Sea*, Vol.15, *Tsunamis*, A. Robinson, E. Bernard (Eds.), Harvard University Press, Cambridge, USA, 201–235.
- MUNK, W.H. (1963), *Some comments regarding diffusion and absorption of tsunamis*, Proc. Tsunami Meet., X Pacific Science Congress, IUGG Monogr. 24, Paris, 53–72.
- MURTY, T.S., NIRUPAMA, N., NISTOR, I., and RAO, A.D. (2005), *Leakage of the Indian Ocean tsunami energy into the Atlantic and Pacific Ocean*, CSEG Recorder, December 2005, 33–36.
- NAGARAJAN, B., SURESH, I., SUNDAR, D. SHARMA, R., LAL, A.K., NEETU, S., SHENOI, S.S.C., SHETYE, S.R., and SHANKAR, D. (2006), *The great tsunami of 26 December 2004: A description based on tide-gauge data from the Indian subcontinent and surrounding areas*, Earth Planets Space 58, 211–215.
- NAKANO, M., and UNOKI, S. (1962), *On the seiches (secondary undulations of tides) along the coast of Japan*, Records Oceanogr. Works Japan Spec. No.6, 169–214.
- OH, I.S., and RABINOVICH, A.B. (1994), *Manifestation of Hokkaido Southwest (Okushiri) tsunami 12 July, 1993, at the coast of Korea*, Sci. Tsunami Hazards 12, 93–116.
- PATTIARATCHI, C.B., and WIJERATNE, E.M.S. (2009), *Tide gauge observations of 2004–2007 Indian Ocean tsunamis from Sri Lanka and Western Australia*, Pure Appl. Geophys. 166, 233–258.

- RABINOVICH, A.B. (2009), *Seiches and harbour oscillations*. In: *Handbook of Coastal and Ocean Engineering* (ed. Y.C. Kim), World Scientific, Singapore, 193–236.
- RABINOVICH, A.B., and STEPHENSON, F.E. (2004), *Longwave measurements for the coast of British Columbia and improvements to the tsunami warning capability*, *Natural Hazards* 32 (3), 313–343.
- RABINOVICH, A.B., and THOMSON, R.E. (2007), *The 26 December 2004 Sumatra tsunami: Analysis of tide gauge data from the World Ocean Part 1. Indian Ocean and South Africa*, *Pure Appl. Geophys.* 164 (2/3), 261–308.
- RABINOVICH, A.B., THOMSON, R.E., and STEPHENSON, F.E. (2006), *The Sumatra tsunami of 26 December 2004 as observed in the North Pacific and North Atlantic Oceans*, *Surv. Geophys.* 27, 647–677.
- RABINOVICH, A., STROKER, K., THOMSON, R., and DAVIS, E. (2011), *DARTs and CORK: High-resolution observations of the 2004 Sumatra tsunami in the abyssal northeast Pacific*, *Geophys. Res. Lett.*, L08502, doi:[10.1029/2011GL047063](https://doi.org/10.1029/2011GL047063).
- SATAKE, K. (1988), *Effects of bathymetry on tsunami propagation: Application of ray tracing to tsunamis*, *Pure Appl. Geophys.* 126 (1), 27–36.
- SATAKE, K., and SHIMAZAKI, K. (1988), *Free oscillations of the Japan Sea excited by earthquakes. II. Modal approach and synthetic tsunamis*, *Geophys. J. R. Astr. Soc.*, 93, 457–463.
- TANIOKA, Y., YUDHIKARA, KUSUSOSE, T., KATHIROLI, S., NISHIMURA, Y., IWASAKI, S.-I., and SATAKE, K. (2006), *Rupture process of the 2004 Great Sumatra-Andaman earthquake estimated from tsunami waveforms*, *Earth Planets Space* 58, 203–209.
- THOMSON, R.E., RABINOVICH, A.B., and KRASSOVSKI, M.V. (2007), *Double jeopardy: Concurrent arrival of the 2004 Sumatra tsunami and storm-generated waves on the Atlantic coast of the United States and Canada*, *Geophys. Res. Lett.* 34, L15607, doi:[10.1029/2007GL030685](https://doi.org/10.1029/2007GL030685).
- TITOV, V.V., RABINOVICH, A.B., MOFJELD, H., THOMSON, R.E., and GONZÁLEZ, F.I. (2005), *The global reach of the 26 December 2004 Sumatra tsunami*, *Science* 309, 2045–2048.
- VAN DORN, W.G.. (1984), *Some tsunami characteristics deducible from tide records*, *J. Phys. Oceanogr.* 14, 353–363.
- VAN DORN, W.G.. (1987), *Tide gage response to tsunamis. Part II: Other oceans and smaller seas*, *J. Phys. Oceanogr.* 17, 1507–1516.
- WILSON, B. (1972), *Seiches*, *Advances in Hydrosociences* 8, 1–94.
- WOODWORTH, P.L., BLACKMAN, D.L., FODEN, P., HOLGATE, S., HORSBURGH, K., KNIGHT, P.L., SMITH, D.E., MACLEOD, E.A., and BRADSHAW E. (2005), *Evidence for the Indonesian tsunami in British tidal records*, *Weather* 60 (9), 263–267.

(Received April 27, 2010, revised July 16, 2010, accepted August 17, 2010, Published online March 2, 2011)